

# Invisible Higgs Decays to Hooperons in the NMSSM

Anja Butter,<sup>1,2</sup> Tilman Plehn,<sup>1</sup> Michael Rauch,<sup>3</sup> Dirk Zerwas,<sup>2</sup> Sophie Henrot-Versillé,<sup>2</sup> and Rémi Lafaye<sup>4</sup>

<sup>1</sup>*Institut für Theoretische Physik, Universität Heidelberg, Germany*

<sup>2</sup>*LAL, CNRS/IN2P3, Orsay Cedex, France*

<sup>3</sup>*Institute for Theoretical Physics, Karlsruhe Institute of Technology (KIT), Karlsruhe, Germany*

<sup>4</sup>*LAPP, Université de Savoie, IN2P3/CNRS, Annecy, France*

The galactic center excess of gamma ray photons can be naturally explained by light Majorana fermions in combination with a pseudoscalar mediator. The NMSSM provides exactly these ingredients. We show that for neutralinos with a significant singlino component the galactic center excess can be linked to invisible decays of the Standard-Model-like Higgs at the LHC. We find predictions for invisible Higgs branching ratios in excess of 50 percent, easily accessible at the LHC. Constraining the NMSSM through GUT-scale boundary conditions only slightly affects this expectation. Our results complement earlier NMSSM studies of the galactic center excess, which link it to heavy Higgs searches at the LHC.

## Contents

<b>I. Introduction and basics</b>	2
A. NMSSM	3
B. Higgs–singlet–singlino sector	3
C. Dark matter annihilation	5
D. Data and tools	6
<b>II. TeV-scale NMSSM</b>	7
A. Galactic center excess	8
B. Invisible Higgs decays	10
<b>III. High-scale NMSSM</b>	14
A. Global analysis	16
B. Galactic center excess	18
<b>IV. Outlook</b>	19
<b>A. Invisible Higgs decays in the MSSM</b>	21
<b>References</b>	22

## I. INTRODUCTION AND BASICS

While the existence of cold dark matter as the main matter component of today's Universe is generally acknowledged, the particle nature of it is still elusive. Searches for dark matter coupled to Standard Model fields with more than a gravitational interaction strength follow three distinct strategies: direct detection, indirect detection, and production at colliders. The latter will receive a significant boost with the start of LHC Run II. The key question is how in the case of weakly interacting dark matter the different search strategies can support and inspire each other. One of the main search strategies for dark matter at the LHC are invisible Higgs decays, most notably in weak boson fusion [1, 2]. For example, in models without new strongly interacting particles such invisible Higgs decays will drive mono-jet searches and are likely to dominate over dark matter pair production in weak boson fusion [3]. In this paper we will reinforce the link between the specific Fermi galactic center excess [4–6] and invisible Higgs decays at the LHC [7, 8] in the framework of the next-to-minimal supersymmetric Standard Model (NMSSM) [9, 10].

The Fermi gamma ray space telescope searches for dark matter signals in its photon spectrum. An excess of gamma rays from the galactic center has for many years avoided possible background interpretations. It can be explained by annihilating dark matter with a spherical distribution around the center of our galaxy. Its spectrum gives preferred mass values for different dark matter candidates. For an annihilation to bottom quarks the preferred mass of the dark matter agent (Hooperon) ranges around 40 GeV [4, 11], extending all the way to 70 GeV [12]. In our analysis of the  $b\bar{b}$  case we will follow Ref. [12] and assume a conservative LSP of 30 GeV to 70 GeV. The cross section should be in the range of  $\sigma v \approx 1.8 \cdot 10^{-26} \text{cm}^3/\text{s}$  [4, 12], with appropriate theoretical or parametric uncertainties for example from the choice of dark matter profile, consistent with the latest Planck thermally averaged results [5]. Such values are intriguingly close to the expectations for a thermally produced weakly interacting dark matter particle (WIMP) [13, 14].

In the MSSM the preferred mass range of the Hooperon is a challenge and typically relies on dark matter annihilation into a pair of gauge boson [15]. In the absence of the highly efficient annihilation through an  $s$ -channel mediator decaying for example into  $b\bar{b}$  pairs the predicted relic density in the Universe tends to be too large. Finding efficient annihilation channels is a serious issue in supersymmetric models [16–18]: first,  $s$ -channel annihilation through the  $Z$ -pole, the SM-like Higgs resonance  $H_{125}$ , or a heavy Higgs resonance are either forbidden by other constraints or too small. Any co-annihilation channel requires an additional supersymmetric particle within 10% of the LSP mass [19–21], which is disfavored by LEP constraints [22]. The way out is an additional mediator, ideally a pseudoscalar with a mass not far above twice the LSP mass [23]. This feature is clearly visible in an analysis in terms of simplified models or effective field theory [24].

As an extension of the MSSM, the NMSSM provides exactly such a mediator, the pseudoscalar part of the singlet/singlino superfield mixed with the MSSM-like pseudoscalar [25]. In the required mass range it will naturally decay to  $b\bar{b}$  pairs, and with a reduced branching ratio to  $\tau^+\tau^-$ . Such an NMSSM setup can be tested in a parameter scan [26] and then linked for example to 4-body Higgs decay [27], trilepton searches at the LHC [28] or even the electroweak phase transition [29]. Because of the structure of the NMSSM we can follow two strategies to accommodate the galactic center excess [30, 31]: first, we can keep the standard bino–Higgsino LSP composition of the MSSM and only couple the neutralinos to the light additional pseudoscalar. Alternatively, we can replace the bino content by a singlino content and assume a singlino–Higgsino, or better bino–singlino–Higgsino LSP. Again, it will couple to the pseudoscalar mediator.

For the bino–Higgsino case the relevant LSP and mediator states are not decoupled from the Standard Model. This means that for example the pseudoscalar mediator can be searched for at the LHC [30]. The singlino–Higgsino channel is more challenging. After introducing the NMSSM singlet/singlino sector and its phenomenology including some useful formulas, in Sec. II A we will study its TeV-scale parameter space linked to the galactic center excess. In Sec. II B we will link the Hooperon parameter space to the size of invisible Higgs couplings. It will turn out that similar to a dark matter Higgs portal [32] the NMSSM interpretation of the galactic center excess will lead to invisible Higgs decays with branching ratios accessible during the upcoming LHC run. In Sec. III we will apply the same criteria to a high-scale NMSSM setup. For this model a global SFITTER likelihood analysis is useful, before we turn to the link between the galactic center excess and invisible Higgs decays.

### A. NMSSM

Compared to the minimal supersymmetric Standard Model the superpotential of the NMSSM [9, 10] includes an additional singlet superfield  $\hat{S}$  and the associated terms

$$W_{\text{NMSSM}} = W_{\text{MSSM}} + \lambda \hat{S} \hat{H}_u \hat{H}_d + \xi_F \hat{S} + \frac{\mu'}{2} \hat{S}^2 + \frac{\kappa}{3} \hat{S}^3, \quad (1)$$

where  $\lambda$  and  $\kappa$  are dimensionless couplings coupling the singlet to itself and to the Higgs bosons. When the singlet acquires a vacuum expectation value  $v_s$ , the Higgs–singlet mixing introduces an effective  $\mu$ -term  $\mu_{\text{eff}} = \lambda v_s$ . The quadratic term proportional to  $\mu'$  is the supersymmetric mass term for the singlet, comparable to the  $\mu$ -term for the MSSM Higgs bosons. Assuming a global supersymmetry the tadpole term proportional to  $\xi_F$  can be removed through a constant shift of the singlet field. Finally, with the help of an ad-hoc  $\mathbb{Z}_3$ -symmetry we can make the superpotential scale invariant and set the one remaining dimensionful parameter,  $\mu'$ , to zero.

The extended superpotential in Eq.(1) in terms of the superfield  $\hat{S}$  can be translated into additional soft-SUSY-breaking terms for the physical singlet field  $S$  [10],

$$-\mathcal{L}_{\text{soft}}^{\text{NMSSM}} = m_S^2 |S|^2 + \left( \lambda A_\lambda H_u H_d S + \frac{\kappa}{3} A_\kappa S^3 + \frac{m_S'^2}{2} S^2 + \xi_S S + \text{h.c.} \right). \quad (2)$$

The  $A_{\lambda,\kappa}$  carry mass dimension and fix the scale of the Lagrangian, while  $\lambda$  and  $\kappa$  defined in Eq.(1) are  $c$ -numbers. An alternative parametrization of the same Lagrangian uses the mass terms  $m_3^2 = B\mu$  and  $m_S'^2 = B'\mu'$ . To be consistent with the  $\mathbb{Z}_3$ -symmetry of the superpotential we also eliminate the corresponding SUSY-breaking terms by setting  $m_3^2 = m_S'^2 = \xi_S = 0$ . In the presence of the effective  $\mu$ -term we can neglect the original  $\mu$  parameter, eliminating yet additional independent scale in the Lagrangian. Correspondingly,  $\mu$  will in the following indicate the effective  $\mu$  term. The relevant NMSSM Lagrangian now reads

$$-\mathcal{L}_{\text{soft}}^{\text{NMSSM}} = m_S^2 |S|^2 + \left( \lambda A_\lambda H_u H_d S + \frac{\kappa}{3} A_\kappa S^3 + \text{h.c.} \right). \quad (3)$$

In the MSSM, the minimization conditions of the Higgs potential can be used to replace  $m_{H_u}^2$  and  $m_{H_d}^2$  by  $m_Z$  and  $\tan\beta$  in the broken phase. Using the additional minimization condition of the NMSSM  $m_S^2$  can be expressed in terms of  $\mu$ . The Higgs–singlet sector [25] is therefore fully described by the parameters  $\lambda, \kappa, A_\lambda, A_\kappa, \mu, \tan\beta$ , and the mass of the  $Z$ -boson.

For specific NMSSM models we have to define the input scale of these parameters. The ratio of the VEVs  $\tan\beta$  is always evaluated at the weak scale  $m_Z$ , because it assumes electroweak symmetry breaking. For the high-scale models discussed in Sec. III  $\lambda, \kappa$  and  $\mu$  are set at the SUSY scale of 1 TeV, while  $A_\lambda$  and  $A_\kappa$  can either be unified to  $A_0$  at the GUT scale or set individually (also at the GUT scale). For the low-scale models in Sec. II all supersymmetric parameters including  $\lambda, \kappa, A_\lambda, A_\kappa, \mu$ , the squark and slepton masses, etc. are set at the SUSY scale.

### B. Higgs–singlet–singlino sector

Compared to the minimal supersymmetric Higgs sector of the MSSM, the phenomenology of the NMSSM is strongly modified by the additional particles, a scalar and a pseudoscalar Higgs bosons and a fifth neutralino. While in general the mass of the singlet states is a free parameter, we will assume that the singlino contributes to a light LSP and that the singlet Higgs states are therefore lighter than their SM-like counterparts. For example, the SM-like Higgs boson with its mass of 125 GeV will typically be the second-lightest CP-even Higgs scalar. For a scale-invariant superpotential we can write out the symmetric Higgs mass matrix [33, 34] in the

$(H, h, S)$ -basis, where  $h$  is the SM-like Higgs boson

$$M_{H,h,S}^2 = m_Z^2 \begin{pmatrix} s_{2\beta}^2 \left(1 - \frac{\lambda^2}{g^2}\right) + \frac{2\mu}{s_{2\beta} m_Z^2} (A_\lambda + \tilde{\kappa}\mu) & c_{2\beta} s_{2\beta} \left(1 - \frac{\lambda^2}{g^2}\right) & -c_{2\beta} \frac{\lambda}{g m_Z} (A_\lambda + \tilde{\kappa}\mu) \\ \cdot & c_{2\beta}^2 + s_{2\beta}^2 \frac{\lambda^2}{g^2} & \frac{2\lambda}{g m_Z} \left(\mu - s_{2\beta} \frac{A_\lambda}{2} + s_{2\beta} \tilde{\kappa}\mu\right) \\ \cdot & \cdot & s_{2\beta} \frac{\lambda^2 A_\lambda}{2g^2 \mu} + \frac{\tilde{\kappa}\mu}{m_Z^2} (A_\kappa + 4\tilde{\kappa}\mu) \end{pmatrix} \quad (4)$$

using the usual notation  $s_\beta = \sin \beta$  and  $c_\beta = \cos \beta$ . In terms of the ordered mass eigenstates  $H_2 \equiv H_{125}$  means that throughout our analysis we identify the second-lightest Higgs with the observed SM-like state. Instead of  $\kappa$  and  $\lambda$ , the modified parameter set

$$\begin{aligned} \tilde{\kappa} &= \frac{\kappa}{\lambda} && \text{(singlet mass parameter)} \\ \frac{\lambda}{g} &&& \text{(singlet decoupling parameter)} \end{aligned} \quad (5)$$

appears in the diagonal entries for the light and heavy MSSM-like Higgs states. In the following, we replace  $\kappa$  with  $\tilde{\kappa}$  but keep  $\lambda$  instead of trivially rescaling it by a constant  $g$ . At tree level the two NMSSM parameters take the pressure off the stop sector for small values of  $\tan \beta$ . In our basis conventions the second Higgs state is the SM-like observed resonance. This means we can decouple the singlet contributions from the observed Higgs. Setting

$$A_\lambda = 2\mu \left( \frac{1}{s_{2\beta}} - \tilde{\kappa} \right) \quad (6)$$

removes the (2,3) entry from the mass matrix and therefore decouples the singlet sector from the SM-like Higgs boson  $h^0$ . Note that this condition does not require any of the couplings in the NMSSM potential of Eq.(3) to vanish.

More generally, we can decouple the singlet from all other Higgs states in the limit  $\lambda \ll g < 1$ . This way the two corresponding entries in the extended Higgs mass matrix vanish. To make the singlet itself heavy we need to increase its entry in the mass matrix in the limit  $\lambda \ll g$ . Neglecting  $A_\kappa$ , the singlet entry in the Higgs mass matrix is  $(2\tilde{\kappa}\mu)^2$ , which for finite  $\kappa$  consistently decouples with the single condition  $\lambda \ll 1$ .

Aside from the extra CP-even Higgs, the singlet extensions of the MSSM Higgs sector adds an additional pseudoscalar. We can transform the weak eigen-basis  $(H_u, H_d, S)$  into a mass basis  $(A, S)$  by a rotation, so that  $A = c_\beta H_u + s_\beta H_d$ . For large values of  $\tan \beta$  the mass eigenstate  $A$  is approximately given by  $H_d$ . Removing the Goldstone modes the  $3 \times 3$  mass matrix in terms of the weak eigenstates can be reduced to a  $2 \times 2$  mass matrix in the basis  $(A, S)$ , which reads

$$M_{A,S}^2 = m_Z^2 \begin{pmatrix} \frac{2\mu (A_\lambda + \tilde{\kappa}\mu)}{s_{2\beta} m_Z^2} & \frac{\lambda}{g m_Z} (A_\lambda - 2\tilde{\kappa}\mu) \\ \cdot & s_{2\beta} \frac{\lambda^2}{g^2} \left( \frac{A_\lambda}{2\mu} + 2\tilde{\kappa} \right) - 3\tilde{\kappa} \frac{\mu A_\kappa}{m_Z^2} \end{pmatrix} \simeq m_Z^2 \begin{pmatrix} \frac{4\mu^2}{s_{2\beta}^2 m_Z^2} & 2 \frac{\lambda}{g m_Z} \frac{\mu}{s_{2\beta}} \\ \cdot & \frac{\lambda^2}{g^2} - 3\tilde{\kappa} \frac{\mu A_\kappa}{m_Z^2} \end{pmatrix}. \quad (7)$$

The pseudoscalar mass eigenstates are denoted as  $A_1$  and  $A_2$ . In the second form we use the singlet decoupling condition Eq.(6) and assume  $s_{2\beta} \ll 1$ . As for the scalar sector, the limit  $\lambda \ll g$  decouples the singlet; its squared mass is then given by  $-3\tilde{\kappa}\mu A_\kappa$ . The upper left entry of the matrix then corresponds to the MSSM pseudoscalar mass,  $m_{A_1}^2 = 2\mu (A_\lambda + \tilde{\kappa}\mu) / s_{2\beta}$ . This way we can choose either this MSSM-like mass or  $A_\lambda$  as input parameter. Similarly, we can replace  $A_\kappa$  with the lower-right entry in  $M_{A,S}^2$  as the input parameter.

Finally, the supersymmetric partner of the singlet field, the singlino appears in the neutralino mass matrix,

$$M_{\tilde{\chi}} = \begin{pmatrix} M_1 & 0 & -m_Z c_\beta s_w & m_Z s_\beta s_w & 0 \\ 0 & M_2 & m_Z c_\beta c_w & -m_Z s_\beta c_w & 0 \\ -m_Z c_\beta s_w & m_Z c_\beta c_w & 0 & -\mu & -m_Z s_\beta \frac{\lambda}{g} \\ m_Z s_\beta s_w & -m_Z s_\beta c_w & -\mu & 0 & -m_Z c_\beta \frac{\lambda}{g} \\ 0 & 0 & -m_Z s_\beta \frac{\lambda}{g} & -m_Z c_\beta \frac{\lambda}{g} & 2\tilde{\kappa}\mu \end{pmatrix} \quad (8)$$

The bottom-right entry indicates that in accordance with Eq.(5) the combination  $2\tilde{\kappa}\mu$  determines the singlino mass. The gauginos do not mix with the singlino. To altogether decouple the singlino, we have to remove the singlino–Higgsino mixing via  $\lambda \ll 1$  and at the same time make the singlino heavy,  $\tilde{\kappa} \gg 1$ . In contrast, for  $\tilde{\kappa} < 1/2$  the LSP will be mostly singlino. In this case the LSP mass  $m_{\tilde{\chi}}$  is approximately given by the solution to

$$\begin{aligned} 2\tilde{\kappa}\mu &= m_{\tilde{\chi}} - m_Z^2 \frac{\lambda^2}{g^2} \frac{m_{\tilde{\chi}} - \mu s_{2\beta}}{m_{\tilde{\chi}}^2 - \mu^2} \\ \Leftrightarrow m_{\tilde{\chi}} &\simeq 2\tilde{\kappa}\mu + \frac{\lambda^2}{g^2} \frac{m_Z^2}{\mu} \frac{2\tilde{\kappa} - s_{2\beta}}{4\tilde{\kappa}^2 - 1}, \end{aligned} \quad (9)$$

so that the LSP mass can be fixed by adjusting  $\tilde{\kappa}$ .

For the interpretation of the galactic center excess a light pseudoscalar will be crucial. To describe its relevant couplings we have to rely on the different mixing matrices. The neutralino mass matrix will be rotated into its mass eigenstates through a matrix  $(N_{ij})$  with  $i, j = 1..5$ . To rotate the pseudoscalar mass matrix into its mass eigenstates we also have to consider the Goldstone mode. The corresponding mixing matrix is  $(P_{ij})$  with  $i = 1, 2$  and  $j = 1, 2, 3$  because the Goldstone is not counted as part of the mass eigenstates  $A_{1,2}$ . The lighter pseudoscalar Yukawa coupling to bottom quarks is given by

$$g_{A_1 bb} = i \frac{m_b}{\sqrt{2} v c_\beta} P_{11}, \quad (10)$$

where  $P_{11}$  is the  $H_d$  component of the lightest mass eigenstate. The coupling to the down-type squarks and sleptons is enhanced by  $1/\cos\beta$ , which is relevant for large  $\tan\beta$ . The coupling mediating the light pseudoscalar decay into the lightest neutralinos is given by

$$\begin{aligned} g_{A_1 \tilde{\chi}\tilde{\chi}} &= \lambda\sqrt{2} (P_{11}N_{14}N_{15} + P_{12}N_{13}N_{15} + P_{13}N_{13}N_{14}) - \lambda\tilde{\kappa}\sqrt{2}P_{13}N_{15}^2 \\ &\quad - (g_1N_{11} - g_2N_{12})(P_{11}N_{13} - P_{12}N_{14}). \end{aligned} \quad (11)$$

When we assign the second Higgs to be SM-like the lightest pseudoscalar will be mainly singlet. Therefore the coupling simplifies to

$$g_{A_1 \tilde{\chi}\tilde{\chi}} = \lambda\sqrt{2} (N_{13}N_{14} - \tilde{\kappa}N_{15}^2), \quad (12)$$

where we set  $P_{11} = P_{12} \ll P_{13} \simeq 1$ . As  $N_{13}$  and  $N_{14}$  differ in sign, both contributions will add up. For a singlino LSP we have sizeable  $N_{15} \rightarrow 1$ , but following Eq.(9)  $\tilde{\kappa}$  ranges around  $m_{\tilde{\chi}}/(2\mu)$ . This means that the singlino term in  $g_{A_1 \tilde{\chi}\tilde{\chi}}$  decreases with increasing  $\mu$ , but the same is true for the Higgsino fractions  $N_{13}$  and  $N_{14}$ . Altogether, a large mediator coupling to the LSP points to a singlino LSP.

### C. Dark matter annihilation

The lightest neutralino being the lightest supersymmetric particle of the NMSSM provides an excellent dark matter candidate. The key constraint for our parameter study will be its relic density assuming thermal production, leaving us with distinct choices of annihilation mechanisms [16, 17]. First, with a dark matter mass

around 40 GeV typical co-annihilation channels [19–21] with particles coupling to the  $Z$ -boson are constrained by  $Z$ -pole measurements at LEP. More generally, they are excluded by direct LEP searches, unless their masses are carefully tuned to only produce soft particles in their production and decays. What is left is neutralino–neutralino annihilation through an  $s$ -channel mediator:

- $Z$ -funnel annihilation through a Higgsino component in the interaction

$$g_{Z\tilde{\chi}\tilde{\chi}} = \frac{g}{2 \cos \theta_W} \gamma_\mu \gamma_5 [N_{13}N_{13} - N_{14}N_{14}] . \quad (13)$$

Because of the velocity dependence of the annihilation rate  $\langle \sigma v \rangle$  this channel usually prefers LSP masses slightly above or below 45 GeV, because directly on the  $Z$ -pole the annihilation is too efficient.

- scalar  $H_{125}$ -funnel annihilation, where the mass of the LSP has to strictly speaking be around 63 GeV. However, in combination with other annihilation channels the  $H_{125}$ -funnel can give the largest contribution already for LSP masses around 55 GeV. The coupling to the Higgs can be found in Eq.(22). The  $H\tilde{\chi}\tilde{\chi}$  coupling will be relevant for invisible Higgs decays, which is why we will discuss it in detail in Sec. II B.
- pseudoscalar  $A$ -funnel annihilation. Unlike in the MSSM we now have a singlet and a Higgs pseudoscalar channel. Both of them can lead to a highly efficient annihilation with  $\sigma v \propto v^0$ . If the pseudoscalar is mainly singlet, the relevant contributions to the neutralino coupling in Eq.(11) reduces to

$$g_{A\tilde{\chi}\tilde{\chi}} = \sqrt{2}\lambda (N_{13}N_{14} - \tilde{\kappa}N_{15}^2) . \quad (14)$$

The Higgsino components differ in sign, so that the absolute value of the couplings add up. Large Higgsino and singlino components therefore lead to a strong coupling.

#### D. Data and tools

In addition to the dark matter relic density and the observed Higgs mass value there exists a wealth of measurements which might constrain supersymmetric models. A large part of the data which we use for our SFITTER parameter study are listed in Tab. I.

The invisible width for  $Z$ -decays,  $\Gamma_{Z \rightarrow \text{inv}}$ , is identified with the additional contribution to the  $Z$ -width from decays into a pair of LSPs. For LSP candidates with a mass smaller than 45 GeV, the LEP results for the  $Z$ -width can be powerful constraints. In addition, we require the lightest chargino to have a mass above 103 GeV, because it is very hard to avoid the LEP2 constraints for charged particle production [22]. This constraint becomes important when we consider regions with small  $\mu < 200$  GeV. If the sum of the lightest CP-even and CP-odd Higgs is smaller than the mass of the  $Z$ -boson, the total width gets an additional contribution. This contribution is compared to the difference between the SM prediction and the measured total width of the

measurement	value and error	
$m_{H_{125}}$	$(125.09 \pm 0.21_{\text{stat}} \pm 0.11_{\text{syst}} \pm 3.0_{\text{theo}})$ GeV	[35, 36]
$\Omega_{\tilde{\chi}} h^2$	$0.1188 \pm 0.0010_{\text{stat}} \pm 0.0120_{\text{theo}}$	[5]
$a_\mu$	$(287 \pm 63_{\text{exp}} \pm 49_{\text{SM}} \pm 20_{\text{theo}}) \cdot 10^{-11}$	[37]
$\text{BR}(B \rightarrow X_s \gamma)$	$(3.43 \pm 0.21_{\text{stat}} \pm 0.07_{\text{syst}}) \cdot 10^{-4}$	[38]
$\text{BR}(B_s^0 \rightarrow \mu^+ \mu^-)$	$(3.2 \pm 1.4_{\text{stat}} \pm 0.5_{\text{syst}} \pm 0.2_{\text{theo}}) \cdot 10^{-9}$	[39]
$\text{BR}(B^+ \rightarrow \tau^+ \nu)$	$(1.41 \pm 0.43_{\text{stat}}) \cdot 10^{-4}$	[40]
$\Delta m_{B^0}$	$(0.510 \pm 0.004_{\text{stat}} \pm 0.003_{\text{syst}} \pm 0.400_{\text{theo}}) \cdot 10^{12} \text{hs}^{-1}$	[40]
$\Delta m_{B_s^0}$	$(17.69 \pm 0.08_{\text{stat}} \pm 7.00_{\text{theo}}) \cdot 10^{12} \text{hs}^{-1}$	[40]
$\Gamma_{Z \rightarrow \text{inv}}$	$(-1.9 \pm 1.5_{\text{stat}} \pm 0.2_{\text{theo}})$ MeV	[41]
$\Gamma_{Z \rightarrow \text{Higgs}}$	$(6.5 \pm 2.3_{\text{stat}} \pm 1.0_{\text{theo}})$ MeV	[41]
$m_t$	$(173.5 \pm 0.6_{\text{stat}} \pm 0.8_{\text{syst}})$ GeV	[42]
$m_{\tilde{\chi}_1^+}$	$> 103$ GeV	[22]
$\sigma_{\tilde{\chi}N}$	direct detection limits	[43]

Table I: Data used for the fit including their systematic and statistical errors from the measurements and theoretical errors for SUSY calculations as far as they are considered.

$Z$ . The mass of the top is an input parameter to the supersymmetric SM-like Higgs. The measurement of  $a_\mu$  can only be satisfied with small slepton masses around 400 GeV or lower. As we decouple the sfermion sector this measurement will only lead to an overall constant contribution to the log-likelihood. Similarly, with the decoupled stop sector the exact value of the SM-like Higgs mass is irrelevant to our analysis, because it can always be re-adjusted independently of our parameters of interest [34]. Finally we also include the Xenon100 [43] limits on direct detection. They are most powerful in the 30 to 100 GeV range, so this measurement will prove to have a strong exclusion power for the scenarios we are interested in.

The Hooperon as an explanation of the galactic center excess [4] is described by two parameters: the LSP mass and the annihilation cross section in the center of the galaxy. For our analysis we will assume the conservative range [12]

$$\begin{aligned} m_{\tilde{\chi}} &= (30 \cdots 70) \text{ GeV} \\ \sigma v &= (0.4 \cdots 10) \cdot 10^{-26} \frac{\text{cm}^3}{\text{s}} \end{aligned} \quad (15)$$

A more detailed analysis in the two-dimensional plane will be part of the full analysis in Sec. II B.

The SFITTER fit then determines multidimensional likelihood maps for the model parameter space. A set of Markov chains selects points in the model space following a Breit–Wigner proposal function. For each point we compute all considered observables and determine a generalized  $\chi^2$  value [44–46]. Theoretical and experimental errors are combined using the RFIT scheme [47], which corresponds to a consistent profiling over the nuisance parameters. Correlations between observables like different channels at the LHC are taken into account. These likelihood maps can be projected on two-dimensional planes as well as single-parameter measurements using profile likelihood or Bayesian methods. Throughout this paper we will apply frequentist profile likelihoods and this way avoid volume effects.

For the TeV-scale fits the same technique is used to select points of the Markov chains following the proposal function. When we display observables instead of the likelihood function, only points that pass sharp criteria, e.g.  $\Omega_{\tilde{\chi}} h^2$  within the theory uncertainties, are displayed. Similar to a profile likelihood, we assign the value of the point with highest likelihood to each bin.

For constraints specifically for the NMSSM we rely on NMSSMTOOLS [48] to calculate the supersymmetric mass spectrum, the Higgs branching ratios, the  $B$  observables,  $(g-2)_\mu$ , and electroweak precision observables. The relic density and the direct detection limits are calculated with MICROMEAS [49]. The number of events in the Higgs production channels at the LHC for the SM-like  $H_{125}$  are computed using the standard SFITTER-Higgs setup [50], HDECAY [51], and NMSSMTOOLS.

For the MSSM study in the appendix the supersymmetric spectrum is calculated using SUSPECT3 [52] while the Higgs branching ratios are computed using SUSY-HIT [51] and HDECAY. For the electroweak precision observables we rely on SUSYPOPE [53]. Finally, we use SUSPECT3 to compute the  $B$ -observables and  $(g-2)_\mu$ . As for the NMSSM the relic density and the direct detection limits are calculated with MICROMEAS.

## II. TEV-SCALE NMSSM

The NMSSM can explain or motivate interesting measurements which are not accessible in the MSSM. This is typically an effect of the extended Higgs particle content, for example including a second pseudoscalar state. One of these measurements is the galactic center excess in gamma rays, based on light neutralinos and a light pseudoscalar mediator. Another is invisible decays of the SM-like Higgs boson. It will turn out that both of them are strongly linked.

We assume a  $\mathbb{Z}_3$ -symmetric NMSSM, where all input parameters are set at the scale 1 TeV. The absence of unifying assumptions leads to a large number of model parameters, namely the slepton and squark masses, the trilinear couplings and the gaugino mass parameters. In this study we decouple the squarks, sleptons, and gluinos by setting the soft masses to 10 TeV and the trilinear couplings to zero, because these sectors are not experimentally relevant. To obtain the correct 125 GeV Higgs mass we adjust the stop masses in the TeV-range appropriately. For the Higgs–singlet sector the relevant input parameters are

$$\{\lambda, \tilde{\kappa}, A_\lambda, A_\kappa, \tan \beta, \mu\}. \quad (16)$$

Alternatively, we can replace  $A_{\lambda,\kappa}$  by the diagonal entries in the pseudoscalar mass matrix of Eq.(7). The neutralino–chargino adds the free parameters  $M_1$  and  $M_2$ .

While  $A_\kappa$  is given at the SUSY scale of 1 TeV, NMSSMTools computes the Higgs masses at the averaged squark masses, in our case around 10 TeV. In Sec. III we will discuss the scale dependence of the singlet related parameters in detail. The approximate form of  $A_\kappa$  at the averaged squark mass scale can be computed from the RGE via

$$\begin{aligned} A_\kappa(10 \text{ TeV}) &= A_{\kappa,0} 10^{\frac{3\lambda\tilde{\kappa}^2}{4\pi^2}} + \left(10^{\frac{3\lambda\tilde{\kappa}^2}{4\pi^2}} - 1\right) \frac{A_\lambda}{\tilde{\kappa}^2} \\ &\approx A_{\kappa,0} + \frac{3 \log 10}{4\pi^2} \lambda A_\lambda. \end{aligned} \quad (17)$$

Due to the large value of  $|A_\lambda|$ , that further increases with the absolute value of  $\mu$ ,  $A_\kappa$  increases from  $-250$  GeV to the order of 30 GeV at 10 TeV for  $\lambda = 0.2$  and  $A_\lambda = 8$  TeV. When we consider small singlet masses, the scale dependence of  $A_\kappa$  plays an important role in their parameter dependence.

### A. Galactic center excess

With the galactic center excess of gamma ray photons we add an experimental motivation for a light neutralino in combination with a light pseudoscalar mediator [4, 24] to the (largely negative) experimental results in Tab I. The spherically symmetric excess can be explained by annihilating dark matter, more specifically by a neutralino in the range of 30 GeV to 40 GeV or even 70 GeV, that annihilates into a pair of fermions, for example  $\tilde{\chi}\tilde{\chi} \rightarrow b\bar{b}$ . For a type-II two-Higgs doublet model the bottom and tau Yukawa couplings are aligned, which means that the assumed decay to a  $b\bar{b}$  pair will dominate over the accompanying decay to  $\tau^+\tau^-$ . In our preferred data regions the  $A_1$  decays into  $b\bar{b}$  (94%) as well as into  $\tau\bar{\tau}$  (6%) pairs, the ratio reflecting the size of the Yukawa couplings and the color factor in the case of quarks.

In the MSSM such a light neutralino LSP is a problem, because it will lead to too large a relic density. In the presence of direct SUSY and Higgs search results there is no obvious way to annihilate it efficiently enough to arrive at the observed relic density. Different co-annihilation channels [19–21] require new charged states in reach of LEP2 and are therefore not viable [22].

In contrast, the two pseudoscalars in the NMSSM can mediate a sufficiently fast annihilation, because the LSP annihilation through its resonance pole is not  $p$ -wave suppressed like it is for vector bosons or scalars. While the mass of the MSSM-like pseudoscalar Higgs is strongly constrained by heavy neutral and charged Higgs searches, the additional light pseudoscalar can be mostly singlet. The neutralino coupling to such a mediator is given in Eq.(11) for a largely singlino mediator turning into Eq.(14).

We consider a generic NMSSM scenario based on a light singlino with a bino and a Higgsino admixture, *i.e.*  $\tilde{\kappa} \ll 1$  [27]. An alternative solution presented in Ref. [30] combines a bino-Higgsino LSP with an NMSSM pseudoscalar mediator, but will not lead to the measurable invisible Higgs decay we are interested in. Light neutralinos with a sizeable wino or Higgsino component are essentially ruled out by  $Z$ -pole measurements and by chargino searches at LEP, so we decouple the wino at  $M_2 = 3$  TeV. In this limit we can link  $\tilde{\kappa}$  to the neutralino mass through Eq.(9). We then adjust  $A_\lambda$  such that the singlet component of the SM-like Higgs is minimized, avoiding Higgs sector constraints altogether [50].

If the annihilation process leading to the galactic center excess proceeds via a pseudoscalar decaying into a pair of bottom quarks, today's dark matter annihilation cross section is [24]

$$\sigma v \Big|_{v=0} \approx \frac{3}{2\pi} \sqrt{1 - \frac{m_b^2}{m_{\tilde{\chi}}^2}} \frac{g_{A_1\tilde{\chi}\tilde{\chi}}^2 g_{A_1bb}^2 m_{\tilde{\chi}}^2}{\left(m_{A_1}^2 - 4m_{\tilde{\chi}}^2\right)^2 + m_{A_1}^2 \Gamma_{A_1}^2}. \quad (18)$$

Large  $\tan\beta$  increases the coupling to the bottom quarks given in Eq.(10). A strong coupling to the bottom quarks also leads to a small width of the light pseudoscalar which further increases the cross section when one is close to the on-shell condition.



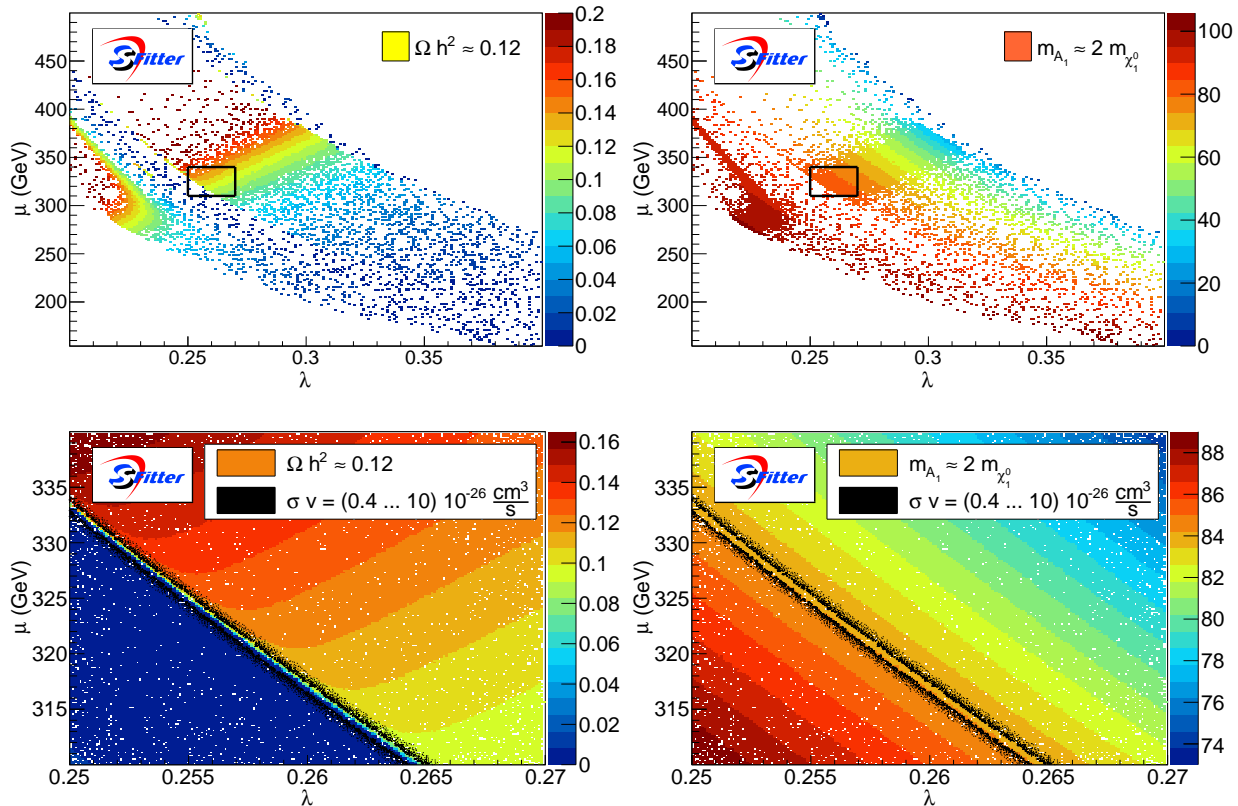


Figure 1: Neutralino relic density (left) and mass of the light pseudoscalar  $A_1$  (right) color-coded as a function of  $\mu$  and  $\lambda$ . The two lower panels are zoomed into the respective upper panels. The orange regions in the lower left panel are compatible with the relic density  $\Omega_{\tilde{\chi}} h^2 = 0.107 \dots 0.131$ , considering the theoretical uncertainty. In addition to the usual decoupling through large scalar masses we fix  $\tan \beta = 40$ ,  $A_\kappa = -250$  GeV,  $A_\lambda$  according to the decoupling condition Eq.(6), and  $\tilde{\kappa}$  corresponding to an LSP mass of 40 GeV through Eq.(9).

Using SFITTER we analyze the NMSSM parameter space with a focus on the SM-like Higgs mass, the LSP mass, the observed relic density  $\Omega_{\tilde{\chi}} h^2$ , the  $Z$  width measurements, the Xenon direct detection constraints, and the galactic center excess. As expected from Sec. IB the key model parameters are the Higgsino mass parameter  $\mu$ , the singlet mass parameter  $\tilde{\kappa}$ , and the coupling  $\lambda$ , which links the singlet to the MSSM Higgs sector. In Fig. 1 we observe a broad band in the  $\lambda$  vs  $\mu$  plane, which is defined by non-zero values for the Higgs masses: for large  $\mu \gg m_Z$  and  $\lambda \rightarrow 1$  the mass of the lightest CP-odd scalar  $A_1$  vanishes. This follows from Eq.(17) and the leading term in Eq.(9), such that the pseudoscalar mass matrix in Eq.(7) only depends on  $\mu$  and  $\lambda$ .  $A_\kappa$  is of the order of 100 GeV at the scale of the averaged squark masses. Following Eq.(17), an increase of  $\lambda$  and  $A_\lambda$ , leads to an increase of  $A_\kappa$ . This results in a smaller mass eigenvalue of  $A_1$ . As  $A_\lambda$  increases with  $\mu$  following Eq.(6), higher values of  $\mu$  lead to smaller pseudoscalar mass.

The mass of the lightest CP-even scalar  $H_1$  is given by the (3, 3) entry of the Higgs mass matrix in Eq.(4) in the Higgs decoupling limit Eq.(6),

$$M_{H,h,S}^2 \Big|_{33} = m_Z^2 \left( \frac{\lambda^2}{g^2} (1 - s_{2\beta} \tilde{\kappa}) + \frac{\tilde{\kappa} \mu}{m_Z^2} (A_\kappa + 4\tilde{\kappa} \mu) \right). \quad (19)$$

$A_\kappa$  enters here with a positive sign, so that for small  $\mu \lesssim m_Z$  and  $\lambda \rightarrow 0$  the mass of this CP-even singlet vanishes. Possible experimental constraints are expected to further reduce this band.

Within this broad band shown in the upper panels of Fig. 1 the structure originates from two sets of input parameters to the calculation of the relic density. On the one hand there is a strong dependence on the mass

of the pseudoscalar mediator, on the other hand the couplings of the LSP depend on the gaugino and Higgsino content of the LSP.

In the upper part of the band, with  $m_{A_1} < 80$  GeV and  $0.26 < \lambda < 0.3$  the dark matter annihilation is mediated by the  $Z$ -funnel, with a coupling to the Higgsino content proportional to  $N_{13}^2 - N_{14}^2$  as given in Eq.(13). Smaller values of  $\lambda$ , correlated with large values of  $\mu$ , decouple the singlet/singlino sector from the MSSM. An efficient dark matter annihilation is not possible, and the relic density is too large. On the other hand, too small values of  $\mu$  and large  $\lambda$  increase the Higgsino–singlino mixing via the off-diagonal terms in the neutralino mass matrix. The Higgsino component in the relic neutralino then results in too small a relic density. In between, Fig. 1 indicates a well-defined regime with the correct relic density. The corresponding mass of the lightest pseudoscalar  $A_1$  indicates that the resonance condition  $m_{A_1} \approx 2m_{\tilde{\chi}}$  is only fulfilled at the lower end of this regime, while the larger part of the allowed band relies on  $Z$ -mediated dark matter annihilation.

In the lower part of the band, defined by the onset of the resonance condition  $m_{A_1} \approx 2m_{\tilde{\chi}}$ , a steep decrease of the relic density leaves a very narrow strip where the annihilation proceeds via the  $A$ -funnel and reproduces the correct value of  $\Omega_{\tilde{\chi}} h^2$ . With the increasing  $A$ -funnel contribution, the  $Z$ -mediated annihilation rate has to decrease, which means that the allowed region bends towards larger values of  $\mu$ . The moment the resonance condition is actually fulfilled, the annihilation through the  $A$ -funnel becomes too efficient, and the predicted relic density drops well below the measured value. For  $m_{A_1} \approx 90$  GeV, corresponding  $\lambda < 0.24$  and  $\mu \approx 300$  GeV, the annihilation again proceeds off-shell, predicting the correct relic density starting with a reduced  $Z$ -mediated rate at large  $\mu$ . At  $\lambda \approx 0.225$  and  $\mu \approx 275$  GeV the annihilation is again mediated by the  $Z$ -boson alone.

A few hardly visible points with the correct relic density at the very top of the allowed mass band arise from  $H_1$ -funnel annihilation and will be of no relevance to our further discussion, because the scalar mediator with its  $p$ -wave suppression fails to explain the galactic center excess.

The lower panels of Fig. 1 focus on  $A_1$ -funnel annihilation just below the resonance condition. There are two regions where the annihilation cross section is compatible with the galactic center excess — within a comparably broad range of  $\sigma v = (0.4 \dots 10) \cdot 10^{-26} \text{ cm}^3/\text{s}$ . The region below the resonance condition  $m_{A_1} \lesssim 2m_{\tilde{\chi}}$  is compatible with the relic density, while the other one is not.

## B. Invisible Higgs decays

Invisible Higgs decays have long been in the focus of LHC studies [1, 2]. At the LHC the upper limits on an invisible branching ratio are 57% in the WBF channel from CMS [8] and 78% combining associated Higgs production and gluon fusion from ATLAS [7]. Eventually, the HL-LHC should be sensitive to invisible branching ratios of a few per-cent in the WBF production channel [2]. Usually, such invisible Higgs decays are associated for example with a Higgs portal to a scalar dark matter sector [32]. We will show that in the NMSSM, invisible Higgs searches can also probe a relevant part of the dark-matter-related parameter space through the decay  $H_{125} \rightarrow \tilde{\chi}\tilde{\chi}$ . Because this decay requires relatively light LSP neutralinos these scenarios can be linked to the galactic center excess discussed in Sec. II A.

The decay width of the CP-even Higgs into two neutralinos is given by

$$\Gamma(H_{125} \rightarrow \tilde{\chi}\tilde{\chi}) = \frac{m_{H_{125}}}{16\pi} g_{H_{125}\tilde{\chi}\tilde{\chi}}^2 \Lambda^{3/2}, \quad \text{with} \quad \Lambda = 1 - \frac{4m_{\tilde{\chi}}^2}{m_H^2}. \quad (20)$$

The Higgs–LSP coupling in the MSSM is

$$g_{H_{125}\tilde{\chi}\tilde{\chi}} \Big|_{\text{MSSM}} = (gN_{11} - g'N_{12}) (\sin \alpha N_{13} + \cos \alpha N_{14}) \\ \equiv (gN_{11} - g'N_{12}) (S_{21}N_{13} + S_{22}N_{14}) . \quad (21)$$

The  $N_{1j}$  are the entries of the neutralino mixing matrix, and  $S_{2i}$  are the entries of the CP-even Higgs mixing matrix. In the simple  $(2 \times 2)$  case the latter are expressed in terms of the mixing angle  $\alpha$ . In the MSSM invisible Higgs decays have to be mediated by gaugino and Higgsino fractions combined, or more specifically

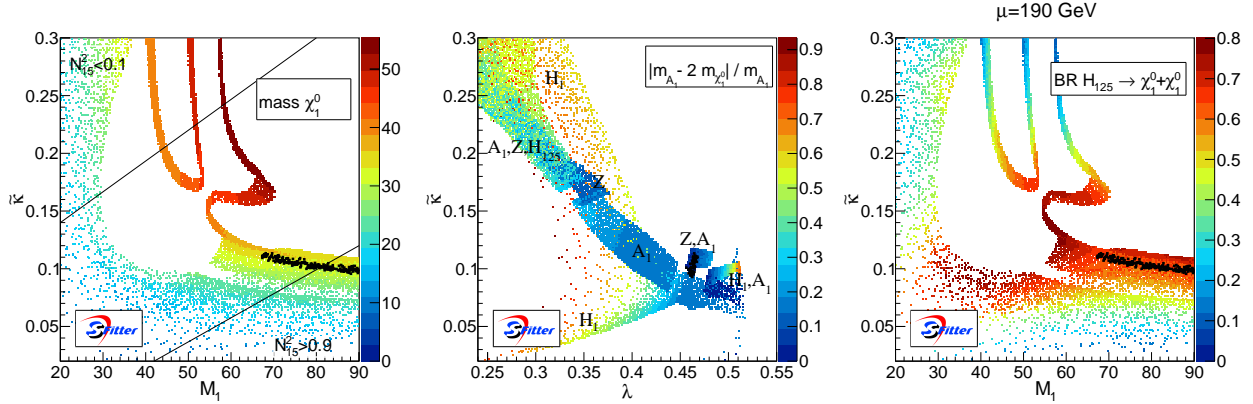


Figure 2: LSP mass, mass splitting between the LSP and the pseudoscalar mediator, and invisible Higgs branching ratio with  $\mu = 190$  GeV and  $A_\kappa = -250$  GeV in the  $\tilde{\kappa} - M_1$ ,  $\tilde{\kappa} - \lambda$ , and  $\tilde{\kappa} - M_1$  planes. All displayed points are compatible with the relic density, Xenon, a chargino mass above 103 GeV, and the correct SM-like Higgs mass. Moreover, they always have an invisible branching ratio  $\text{BR}(H_{125} \rightarrow \tilde{\chi}\tilde{\chi}) > 10\%$ . The black points are consistent with the galactic center excess.

by a mixed bino–Higgsino LSP. In the NMSSM this coupling receives additional contributions from the singlet, namely

$$g_{H\tilde{\chi}\tilde{\chi}} = g_{H\tilde{\chi}\tilde{\chi}} \Big|_{\text{MSSM}} + \sqrt{2}\lambda [(S_{21}N_{14} + S_{22}N_{13})N_{15} + S_{23}N_{13}N_{14} - \tilde{\kappa}S_{23}N_{15}^2] . \quad (22)$$

Now, invisible Higgs decays can proceed to bino–Higgsino, singlino–Higgsino, and in the presence of a singlet component in the Higgs boson even pure Higgsino and pure singlino LSPs.

Just like the galactic center excess, invisible decays of the SM-like Higgs benefit from a light, mixed neutralino LSP. Decoupling squarks, sleptons, and gluino we can ask if there are regions with a large branching ratio  $H_{125} \rightarrow \tilde{\chi}\tilde{\chi}$  for a mixed bino–Higgsino–singlino LSP, and such parameter regions can be related to the galactic center excess.

Following Eq.(9) the mass of the singlino LSP is given by  $2\mu\tilde{\kappa}$ . To suppress the Higgsino component we require  $\tilde{\kappa} < 1/2$  and keep  $\mu > 190$  GeV in a first step. This way the Higgsino component in the LSP ranges around 5% to 10%, leading to a sizeable coupling to the Higgs sector but preventing a large coupling to the  $Z$ -boson. Our choice of parameters for the galactic center excess fixes  $\tan\beta = 40$  and  $A_\kappa < -250$  GeV. The coupling condition Eq.(6) determines  $A_\lambda$  to minimize the singlet component of the SM-like Higgs. The remaining parameters are  $\lambda$ ,  $\tilde{\kappa}$  and  $M_1$ . Small values of  $M_1$  increase the bino component of the LSP while small values of  $\tilde{\kappa}$  increase the singlino component. To keep a constant hooperon mass,  $\tilde{\kappa}$  and  $M_1$  have to behave inversely proportional.

In Fig. 2 we show the result of the SFITTER analysis, starting with fixed  $\mu = 190$  GeV. Of the experimental constraints discussed in Sec. ID we now only include the relic density, the Xenon constraints, the chargino mass constraints, the invisible  $Z$ -width constraint  $\Gamma_{Z \rightarrow \text{inv}} < 2$  MeV and the SM-like Higgs mass constraint  $m_H = 122 \dots 128$  GeV. We only show parameter points with  $\text{BR}(H_{125} \rightarrow \tilde{\chi}\tilde{\chi}) > 10\%$ . For our starting value  $\mu = 190$  GeV we fix  $A_\kappa = -250$  GeV.

Three distinct, narrow strips for example in the upper row of Fig. 2 are defined by constant LSP masses around 40 GeV, 48 GeV, and 55 GeV. For  $m_{\tilde{\chi}} \approx 55$  GeV the annihilation is mediated by  $H_{125}$ . If the mass moves closer to the  $H_{125}$  on-shell condition the relic density becomes too small. At the lower end of the 55 GeV strip the additional annihilation through the  $A_1$  pseudoscalar and the  $Z$  becomes too strong to reproduce the observed relic density. Numerically, the reason is that  $m_{A_1} \propto \tilde{\kappa}$  reaches 120 GeV around  $\tilde{\kappa} = 0.16$ , which opens a pseudoscalar-mediated LSP annihilation channel. For  $\mu = 190$  GeV this coincides with the possibility to efficiently annihilate through an  $s$ -channel  $Z$ -exchange.

The 40 GeV and 48 GeV strips are defined by the  $Z$ -mediated LSP annihilation. Each of them lives on one side of the  $Z$ -pole, because the annihilation on the pole is too efficient to give the correct relic density. Both strips follow the asymptotic behavior of the LSP mass. The 40 GeV strip continues towards high values of  $M_1$ , but with a reduced LSP mass. The reason is that the additional annihilation mediated by  $A_1$  adds to  $Z$ -mediated annihilation. Finally, the annihilation via the pseudoscalar connects the annihilation channels for  $m_{\tilde{\chi}} = 48$  GeV and  $m_{\tilde{\chi}} = 55$  GeV around  $M_1 = 70$ .

In the broad regions with  $M_1 = 10 \dots 40$  GeV the annihilation is in addition mediated by  $H_1$  ( $\tilde{\kappa} > 0.1$ ) and by a combination of  $H_1$  and  $A_1$  ( $\tilde{\kappa} < 0.1$ ).

One key feature is the hole in the allowed parameter space around  $\tilde{\kappa} = 0.15$  and  $M_1 = 50$  GeV. For example along the 40 GeV strip the LSP composition changes from bino to singlino, with a 5% to 12% Higgsino contribution. While the sum of the two Higgsino components increases towards the singlino LSP, their ratio switches. This leads to an intermediate region where both components have a similar value. At this point  $g_{Z\tilde{\chi}\tilde{\chi}}$  given by Eq.(13) vanishes, interrupting the  $Z$ -mediated annihilation. The other annihilation channels are weak, so the relic density is too large.

In the right panel of Fig. 2 we see that the parameter points which can account for the galactic center excess appear precisely where we also expect invisible decays for the SM-like Higgs  $H_{125}$ . Indeed, for  $M_1 = 50 \dots 60$  GeV and  $\tilde{\kappa} \approx 0.1$  we find the highest branching ratio  $H_{125} \rightarrow \tilde{\chi}\tilde{\chi}$ . This region has unique properties: as discussed above, the dark matter annihilation proceeds through an on-shell  $Z$ -boson, with  $m_{\tilde{\chi}} = 45 \pm 2$  GeV. The LSP is a mixed state with 8% Higgsino, 30% to 50% singlino, and 40% to 50% bino content. The two Higgsino components are of the same size, strongly reducing the  $Z$ -coupling  $g_{Z\tilde{\chi}\tilde{\chi}}$ . The lightest pseudoscalar  $A_1$  has a mass around 115 to 135 GeV, but as an at least 95% singlet remains undetected. Because of the strongly mixed LSP content, each  $N_{1i}$  term can contribute to  $g_{H_2\tilde{\chi}\tilde{\chi}}$ . This large value induces an invisible branching ratio of up to\*.

$$\text{BR}(H_{125} \rightarrow \tilde{\chi}\tilde{\chi}) \lesssim 70\% \quad \text{for } \mu = 190 \text{ GeV}, \quad (23)$$

for the parameter space consistent with the galactic center excess.

In this region with an overwhelming invisible Higgs decay width we need check a few experimental constraints not represented in Fig. 2: First, the cancellation of the two Higgsino components renders the partial decay width  $\Gamma_{Z \rightarrow \text{inv}}$  smaller than 0.1 MeV. For a mostly-singlino LSP region it increases through large  $N_{14}$  values up to 2 MeV. The Xenon limits on direct dark matter detection exclude the region centered around  $M_1 = 40$  GeV and  $\tilde{\kappa} = 0.2$ , linked to the  $H_1$  and  $A_1$  annihilation channels. However, none of these additional constraints affect the parameter regions with invisible Higgs branching ratios between 10% and 30%.

In the next step we vary  $\mu$ , and with it  $A_\kappa$  to keep the singlet Higgs masses in the desired range. This means that for  $\mu = 220$  GeV and  $\mu = 320$  GeV we have to set  $A_\kappa = -280$  GeV and  $A_\kappa = -350$  GeV, respectively.

Increasing  $\mu$  slowly impacts the LSP annihilation channels. First, we see that the allowed regions for  $\mu = 220$  GeV shown in the upper left panel of Fig. 3 are very similar the case of  $\mu = 190$  GeV. This indicates that our above results are not very fine-tuned. For a fixed LSP mass an increase of  $\mu$  merely leads to a smaller Higgsino component, which in turn leads to a smaller  $Z\tilde{\chi}\tilde{\chi}$  coupling. It also decreases the invisible Higgs branching to

$$\text{BR}(H_{125} \rightarrow \tilde{\chi}\tilde{\chi}) \lesssim 40\% \quad \text{for } \mu = 220 \text{ GeV}, \quad (24)$$

in the relevant parameter region for the galactic center excess.

For larger  $\mu = 320$  GeV the picture changes: for a fixed LSP mass an increase of  $\mu$  leads to a smaller Higgsino content. While for  $\mu = 190$  GeV the two Higgsino components add to 5% ... 17%, they now stay in the 2% ... 5% range. This immediately leads to a smaller  $Z\tilde{\chi}\tilde{\chi}$  coupling — and a reduced invisible Higgs branching ratio. The  $Z\tilde{\chi}\tilde{\chi}$  coupling implies that the LSP mass has to be closer to the on-shell condition to give the correct relic density. Indeed, for a bino-like LSP and  $\mu = 320$  GeV, the lowest mass strip is now defined by  $m_{\tilde{\chi}} \approx 42$  GeV

---

\* In this discussion we ignore the limits on invisible Higgs decays for example from the SFITTER Higgs analysis [54]. There, we find  $\text{BR}_{\text{inv}} < 30.6\%$  at 95% C.L. in an 8-parameter coupling analysis. For a dedicated NMSSM fit this limit is expected to be even more constraining.

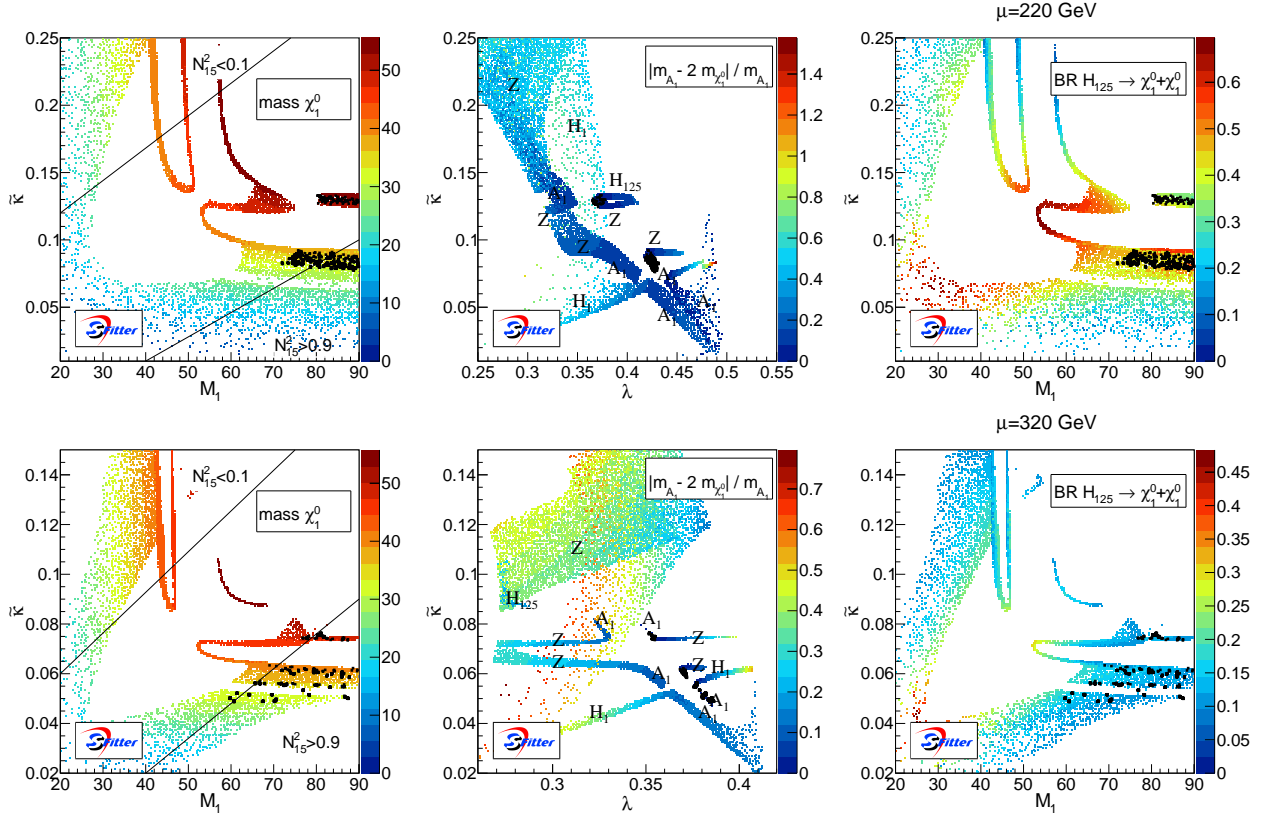


Figure 3: LSP mass, mass splitting between the LSP and the pseudoscalar mediator, and invisible Higgs branching ratio now for  $\mu = 220$  GeV (upper row) and  $\mu = 320$  GeV (lower row) in the  $\tilde{\kappa} - M_1$ ,  $\tilde{\kappa} - \lambda$ , and  $\tilde{\kappa} - M_1$  plane. Correspondingly we choose  $A_\kappa = -280$  GeV and  $-380$  GeV. As in Fig. 2 all displayed points are compatible with the relic density, Xenon, a chargino mass above 103 GeV, and the correct SM-like Higgs mass. Moreover, they always have an invisible branching ratio  $\text{BR}(H_{125} \rightarrow \tilde{\chi}\tilde{\chi}) > 10\%$ . The black points are consistent with the galactic center excess.

instead of 40 GeV. Similarly, the high-mass strip moves down from  $m_{\tilde{\chi}} = 48$  GeV to 46 GeV. Altogether, in the lower left panel of Fig. 3 we see that the annihilation regions mediated by the  $Z$ -funnel and the  $H_1$  funnel with  $m_{\tilde{\chi}} = 55$  GeV clearly separate.

The annihilation processes can now best be identified in the central lower panel of Fig. 3, showing the correlation between  $\tilde{\kappa}$  and  $\lambda$ . Annihilation through a  $Z$ -boson occurs in the two parallel strips with  $\tilde{\kappa} \approx 0.065$  and  $\tilde{\kappa} \approx 0.07$ . They are divided by the actual on-shell condition  $2m_{\tilde{\chi}} = m_Z$ , for which LSP annihilation becomes too efficient.

Following Eq.(4) and replacing  $A_\lambda$  through Eq.(6) we see that the  $H_1$  mass increases with  $\lambda$  directly, as well as indirectly via  $A_\kappa$ . Larger values of  $\lambda$  lead to a steeper increase of the scale dependence and thereby increases  $A_\kappa$  at the 10 TeV scale. At the same time the neutralino mass increases with  $\tilde{\kappa}$ . This explains why for an annihilation via  $H_1$  we find a strip increasing from  $\tilde{\kappa} \approx 0.02$  and  $\lambda \approx 0.24$  to  $\tilde{\kappa} \approx 0.06$  and  $\lambda = 0.4$

For the galactic center excess the annihilation via the pseudoscalar  $A_1$  is crucial. The LSP mass decreases with  $\kappa$ , while the mediator mass  $m_{A_1}$  decreases with  $\lambda$ . This is caused by the renormalization group running, which for larger  $\lambda$  pushes  $A_\kappa$  to larger values at 10 TeV. Following Eq.(7) the pseudoscalar mass includes a factor  $-A_\kappa$ , which means it indeed decreases with increasing  $\lambda$ . To maintain the relation between the LSP and mediator masses,  $\lambda$  and  $\tilde{\kappa}$  have to be anti-correlated. This is what we observe in the two  $A_1$ -mediated strips in the central lower panel of Fig. 3. These strips with the efficient pseudoscalar mediator also accommodate the galactic center excess, as expected from the simplified model analysis [24]. Again, as before the  $A_1$ -mediated annihilation blends in with  $Z$ -mediated annihilation.

For  $\mu = 320$  GeV we find an increasingly small number of parameter points which accommodate the galactic

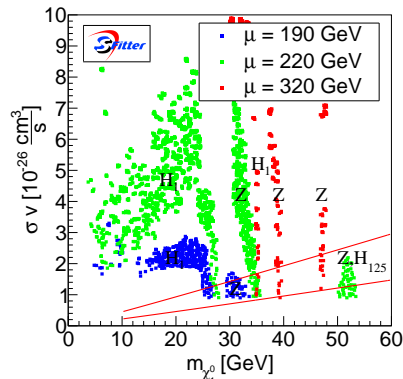


Figure 4: Correlation between the LSP mass and the dark matter annihilation rate for our three reference points in  $\mu$ , to be compared to for example Fig. 3 in Ref. [12]. The lines correspond to the two sigma limits there. If available, we indicate the leading LSP annihilation channels. Points with  $m_{\tilde{\chi}} < 30$  GeV shown in this figure are not included in our analysis and in Figs. 2 and 3.

center excess as well as the current relic density. However, they reside in a regime with

$$\text{BR}(H_{125} \rightarrow \tilde{\chi}\tilde{\chi}) \lesssim 15\% \quad \text{for } \mu = 320 \text{ GeV} , \quad (25)$$

again consistent with the galactic center excess. One aspect which will become relevant when we embed the NMSSM in a unified framework at the GUT scale is the  $M_1$ -dependence of the Hooperon-compatible parameter points. For all three  $\mu$ -values we observe a tail towards large  $M_1$  values, for which the LSP properties do not change any longer. While we do not show values above  $M_1 > 90$  GeV, we could extend the curves to much larger bino masses.

For a combination of the different  $\mu$  values assumed in the above analysis we show the two-dimensional correlations between the LSP mass and the annihilation rate in Fig. 4. The valid NMSSM parameter points include LSP masses below 30 GeV, which we do not consider in our analysis of the invisible branching fractions [4, 12]. We see that most of the NMSSM points would prefer a larger annihilation rate than the central Hooperon value, but this annihilation rate can be accommodated by moving the different masses slightly on and off the respective resonance conditions. Moreover, the majority of allowed points have LSP masses between 10 and 30 GeV, in particular for  $\mu = 220$  GeV. On the other hand, for all three values of  $\mu$  it is possible to enter the preferred region taken from Ref. [12] in the two-dimensional  $\sigma v$  vs  $m_{\tilde{\chi}}$  plane.

### III. HIGH-SCALE NMSSM

Instead of using the full set of TeV-scale model parameters we can require the NMSSM to fulfill a set of unification assumptions at large energy scales. We start with a unified squark and slepton mass  $m_0$ , a unified gaugino mass  $m_{1/2}$ , and a unified trilinear coupling  $A_0$  at the GUT scale [55]. Furthermore, we require a  $\mathbb{Z}_3$ -symmetry to remove for example the  $\mu$ -term and replace it with an effective  $\mu$ -term induced by the singlet VEV. Because we do not require unified Higgs masses  $m_{H_u}^2, m_{H_d}^2$ , and  $m_S^2$  we refer to the model as the NUH-NMSSM (non-universal Higgs masses) [56].

From Sec. IB we know that to produce a light scalar and a light pseudoscalar,  $\tilde{\kappa}$  has to be small and  $A_\kappa$  evaluated at 10 TeV has to range around the electroweak scale. The running of the different model parameters from the GUT scale to the weak scale is described by renormalization group equations, for example for the

singlet couplings

$$\begin{aligned}
16\pi^2 \frac{d\lambda}{d\log Q^2} &= \frac{\lambda}{2} (4\lambda^2 + 3h_t^2 + 3h_b^2 + h_\tau^2 + 2\kappa^2 - g_1^2 - 3g_2^2) \\
16\pi^2 \frac{d\kappa}{d\log Q^2} &= \frac{\kappa}{2} (6\lambda^2 + 6\kappa^2) \\
16\pi^2 \frac{d\tilde{\kappa}}{d\log Q^2} &= \frac{\tilde{\kappa}}{2} (4\tilde{\kappa}^2\lambda^2 + 2\lambda^2 - 3h_t^2 - 3h_b^2 - h_\tau^2 + g_1^2 + 3g_2^2) .
\end{aligned} \tag{26}$$

The Yukawa couplings are defined as  $m_f = h_f v \sin \beta / \sqrt{2}$ . The couplings  $\kappa$  and  $\lambda$  appear squared, so that for a choice of signs our argument will hold for their absolute values. If we neglect the gauge couplings,  $\lambda$  increases with  $Q$  and runs into a Landau pole. If we also neglect the Yukawas, which accelerate this increase, the Landau pole is approximately given by

$$\lambda(Q) = \lambda_0 \left[ 1 - \frac{\lambda_0^2}{2\pi^2} \log \frac{Q}{Q_0} \right]^{-1/2} \rightarrow \infty . \tag{27}$$

For our theory to be valid up to  $Q = 10^{16}$  GeV the Higgs–singlet coupling is limited to  $\lambda_0 < 0.81$  at  $Q_0 = 1$  TeV. The large and also increasing top Yukawa coupling further accelerates the approach of a strongly interacting regime, requiring  $\lambda_0 \lesssim 0.5 \dots 0.6$  for a valid theory to the GUT scale. Assuming roughly constant  $\lambda$  and also ignoring the Standard Model Yukawa and gauge couplings, the running singlet self-coupling  $\kappa$  is given by

$$\kappa(Q) = \kappa_0 \left[ 1 + \kappa_0^2 \left( 1 - \left( \frac{Q}{Q_0} \right)^{\frac{3\lambda^2}{4\pi^2}} \right) \right]^{-1/2} \left( \frac{Q}{Q_0} \right)^{\frac{3\lambda^2}{8\pi^2}} . \tag{28}$$

The maximum value of  $\kappa$  for which the theory is defined up to  $Q = 10^{16}$  GeV ranges around

$$\kappa_{\max} = \frac{1}{\sqrt{\left( \frac{Q}{Q_0} \right)^{\frac{3\lambda^2}{8\pi^2}} - 1}} = \begin{cases} 0.66 & \lambda = 0 \\ 0.53 & \lambda = 0.6 . \end{cases} \tag{29}$$

In this approximation we can compute a few example values by iterating: starting with  $\lambda = 0.3 = \kappa_0$  at the TeV scale we find  $\kappa = 0.43$  and  $\lambda = 0.61$  at  $10^{16}$  GeV. The singlet mass parameter  $\tilde{\kappa}$  decreases from 1.0 to 0.7.

In the running of  $\tilde{\kappa}$  the top Yukawa coupling enters with a negative sign. Therefore  $\kappa$  increases slower with the scale than  $\lambda$  as long as  $\kappa, \lambda \ll h_t$ . If we consider larger values as weak-scale starting points,  $\kappa$  increases faster than  $\lambda$ .  $\lambda = 0.45 = \kappa_0$  gives  $\kappa = 1.7$  and  $\lambda = 1.2$  at the GUT scale, so  $\tilde{\kappa}$  increases from 1.0 to 1.4.

For the component fields both, the Higgs–singlet coupling and the singlet self-coupling come with associated mass scales. They run like

$$\begin{aligned}
16\pi^2 \frac{dA_\lambda}{d\log Q^2} &= 4\lambda^2 A_\lambda + 3h_t^2 A_t + 3h_b^2 A_b + h_\tau^2 A_\tau + 2\kappa^2 A_\kappa + g_1^2 M_1 + 3g_2^2 M_2 \\
16\pi^2 \frac{dA_\kappa}{d\log Q^2} &= 6\lambda^2 (\tilde{\kappa}^2 A_\kappa + A_\lambda) \\
16\pi^2 \frac{dm_S^2}{d\log Q^2} &= 2\lambda^2 (m_{H_u}^2 + m_{H_d}^2 + m_S^2 + A_\lambda^2 + 3\tilde{\kappa}^2 m_S^2 + \tilde{\kappa}^2 A_\kappa^2)
\end{aligned} \tag{30}$$

The increase of these mass scales towards high energy scales clearly does not help with the appearance of a strongly interacting Higgs–singlet sector in the NMSSM.

Finally, we can ask how the new NMSSM Higgs–singlet parameters affect the running of the MSSM-like parameters. An interesting parameter in the MSSM is the stop mixing parameter, which now runs like

$$16\pi^2 \frac{dA_t}{d\log Q^2} = 6h_t^2 A_t + h_b^2 A_b + \lambda^2 A_\lambda + \frac{13}{9} g_1^2 M_1 + 3g_2^2 M_2 + \frac{16}{3} g_3^2 M_3 \tag{31}$$

While there will be an effect of the additional singlet on the running of the MSSM-like parameters, its impact will be numerically small. The only exception appears when we allow with Higgs-singlet sector to become strongly interacting at relatively low scales, in which case for example the stop mixing parameter will also sharply increase.

### A. Global analysis

From the previous discussion it is clear that there are several, more or less distinct regions of the NMSSM parameter space, which allow us to describe the Hooperon. This is less clear when we constrain the model parameters through unification assumptions. Most notably, the unification of the gaugino masses at the GUT scale links the bino mass  $M_1$  to the gluino mass, which in turn is constrained by LHC searches [57].

Before we focus on the galactic center excess and invisible Higgs decays, it makes sense to test how well the unified NUH-NMSSM can accommodate all other available data listed in Tab. I, including the observed relic density and the Xenon limits on direct detection. We also include the SM-like Higgs couplings strengths from the SFITTER-Higgs analysis [50]. Our parameters of interest are  $\lambda$ ,  $\tilde{\kappa}$ , and  $\mu$ .

In the NUH-NMSSM with decoupled scalars ( $m_0 = 2$  TeV) we face two major differences compared to the TeV-scale model. First, unification links the binos mass  $M_1$  to the gluino mass, which is constrained by direct LHC searches [57]. In addition, the SUSY-breaking singlet parameters  $A_\lambda$  and  $A_\kappa$  are set at the GUT scale. This means that we cannot apply the simple decoupling relations for example given in Eq.(6).

To get some control over the parameters we start with an SFITTER likelihood analysis, for example to see how the requirement  $H_2 = H_{125}$  translates into the high-scale parameters  $A_\lambda, A_\kappa, m_{1/2}$ , and  $A_0$ . The unified gaugino mass is proportional to the gluino mass and hence constrained to be  $m_{1/2} \gtrsim 500$  GeV. The mass scales  $A_\lambda$  and  $A_\kappa$  will eventually be constrained by the requirement of a light scalar mass, and we fix their ranges to  $A_\kappa = -1.5 \dots 1.5$  TeV and  $A_\lambda = -1 \dots 5$  TeV. From our experience with the TeV-scale NMSSM we limit the singlet parameters, still defined at 1 TeV, to  $\lambda < 1$ ,  $\kappa < 1$ , and  $\mu < 400$  GeV. The ratio of the VEVs is fixed again to  $\tan \beta = 40$ .

As before, we use all data listed in Tab. I. In the Higgs sector we identify the observed SM-like Higgs with the second-lightest NMSSM Higgs and include the Higgs couplings measurements from ATLAS and CMS searches [50]. A set of two-dimensional profile likelihood projections is displayed in Fig. 5.

The upper left panel shows the profile likelihood projection on the  $\tilde{\kappa} - \lambda$  plane. We identify three distinct regions through their dark matter annihilation channels [16]:

1. a broad band with  $\tilde{\kappa} = 0.1 \dots 0.3$ ,  $\lambda < 0.25$ , and  $\mu = 90 \dots 200$  GeV. It includes two LSP mass regions with an annihilation through  $Z$ - and  $H_{125}$ -exchange.
2. a narrow strip around  $\tilde{\kappa} \approx 0.42$ ,  $\lambda < 0.2$ , and  $\mu = 90 \dots 350$  GeV. It relies on a light chargino either for co-annihilation or for  $t$ -channel exchange for efficient dark matter annihilation.
3. a bulk region with  $\tilde{\kappa} = 0.3 \dots 0.7$ ,  $\lambda > 0.2$ , and  $\mu = 90 \dots 150$  GeV. Here, the annihilation occurs through a mix of channels, notably including the light singlet pseudoscalar.

The transition between the second and third region is not uniquely defined, but involves it the appearance of the  $A_1$ -funnel annihilation and a drop in the LSP singlino content from 70% ... 90% to 10% ... 70%. Following Sec. IIB, an invisible branching ratio needs a LSP mass smaller than 62 GeV. Therefore the only region compatible with the galactic center excess and an invisible branching ratio will be  $\tilde{\kappa} = 0.1 \dots 0.25$ .

The upper right panel in Fig. 5 shows the profile likelihood projection on the  $\tilde{\kappa} - \mu$  plane. A lower bound  $\mu > 90$  GeV arises from the chargino mass limit. An upper bound is connected to the requirement that the second-lightest NMSSM Higgs be the SM-like state: the mass of the singlet-like Higgs is proportional to  $\mu$ , so for large  $\mu$  it approaches 125 GeV. This translates into the globally observed  $\mu < 400$  GeV.

We then combine the range in  $\mu$  with the  $m_{1/2}$  dependence. As mentioned before, the gluino bound sets a lower limit on  $m_{1/2} > 500$  GeV. The combination of  $\mu < 400$  GeV and  $m_{1/2} > 500$  GeV results in a sum of the bino and wino LSP components to be less than 1% throughout the plane. The mass and composition of the Higgsino-singlino LSP is set by  $\mu, \tilde{\kappa}$ , and  $\lambda$ . For  $\tilde{\kappa} > 0.5$  it is mainly Higgsino, with its mass set by  $\mu$ . For



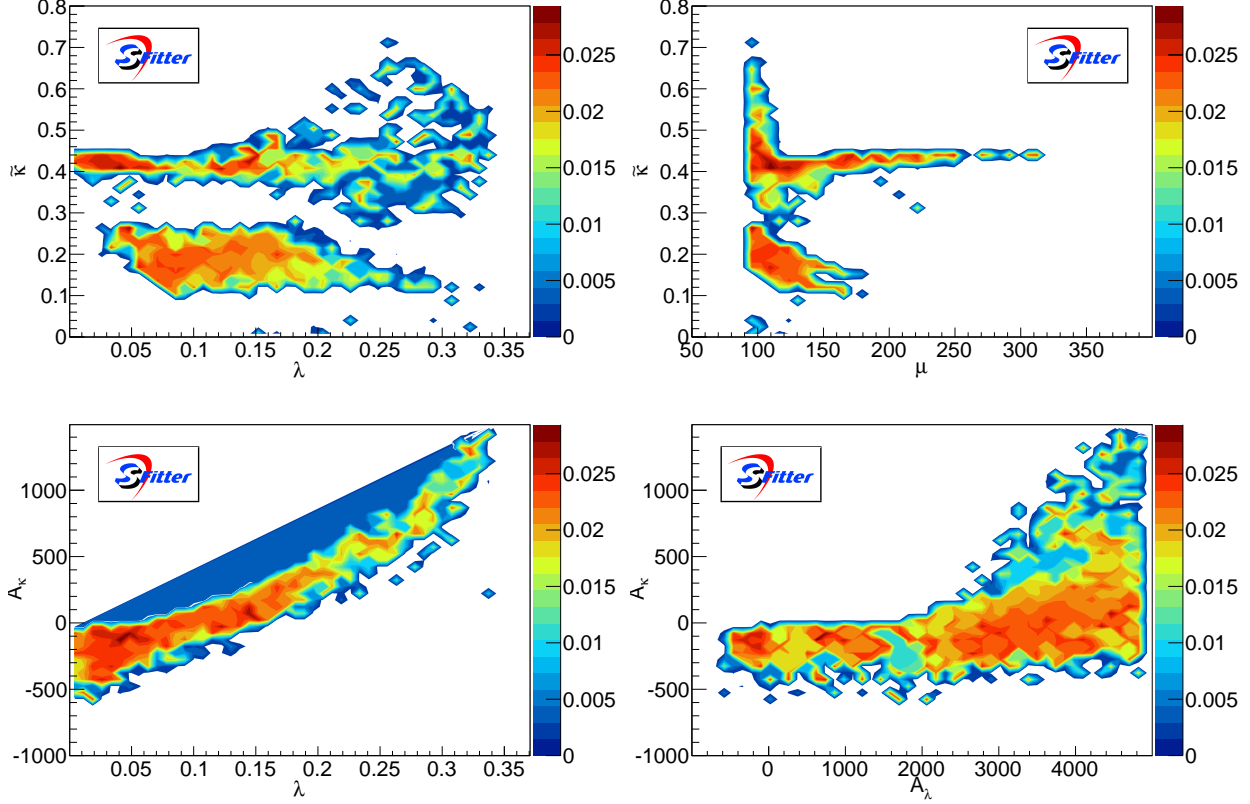


Figure 5: Profile likelihood projections of the NUH-NMSSM assuming a SM-like  $H_2 \equiv H_{125}$ . All measurements shown in Tab. I and the SM-like Higgs couplings [50] are included. Of the shown parameters  $A_\kappa$ , and  $A_\lambda$  are defined at the GUT scale. The singlet parameters  $\lambda$ ,  $\tilde{\kappa}$  and  $\mu$  are defined at 1 TeV, just like in the low scale scenario.

$\tilde{\kappa} < 0.4$  the LSP is mainly singlino, and following Eq.(9) its mass is given by  $2\tilde{\kappa}\mu$ . Large values of  $\lambda$  lead to a stronger mixing between singlino and Higgsino.

Of the list of regions introduced above we first consider the band with  $\tilde{\kappa} = 0.1 \dots 0.3$ , where the singlino component is larger than 85%. The corresponding values of  $\mu$  range from 90 GeV to 200 GeV, resulting in two regions of neutralino mass compatible with the measured relic density: for  $m_{\tilde{\chi}} = 40 \dots 50$  GeV the annihilation is mediated by a  $Z$ -boson, while for  $m_{\tilde{\chi}} = 55 \dots 60$  GeV the LSP annihilates via the SM-like Higgs into  $b\bar{b}$  and partially into light Higgs bosons. Annihilation via the lightest pseudoscalar, as relevant for the galactic center excess can occur, but it is not a main annihilation channel.

In the narrow second strip, the higher value of  $\tilde{\kappa} = 0.42$  leads to a smaller Higgsino component, that varies between 70% and 90%. The higher value of  $\tilde{\kappa}$  leads to a mass ratio of about 0.85 between the LSP and the Higgsino-like chargino. This opens the chargino co-annihilation channel or neutralino annihilation into  $WW$  and  $ZZ$  through a chargino in the  $t$ -channel. In the upper right panel we can verify that this channel is open up to  $\mu = 350$  GeV.

Finally, for  $\lambda > 0.2$  the different annihilation processes are no longer well separated. Inversely correlated to  $\tilde{\kappa} = 0.3 \dots 0.7$  the singlino component decreases from 70% to 10%. For this region we find an upper bound of  $\mu < 150$  GeV, resulting in neutralino masses between 60 and 100 GeV. For neutralinos around 60 GeV the annihilation proceeds via the SM-like Higgs, while for larger masses the annihilation channel is a mixture of a pseudoscalar funnel, chargino co-annihilation, and  $t$ -channel annihilation via a chargino.

The lower panels of Fig. 5 show the profile likelihood projection onto the  $\lambda - A_\kappa$  and the  $A_\lambda - A_\kappa$  planes. From Eq.(4) and Eq.(7) we know that the scalar and pseudoscalar singlet mass terms increase with  $\lambda$ . The singlet-like scalar has to remain lighter than 125 GeV, leading to an upper limit on  $\lambda$  depending on  $A_\kappa$  and

$A_\lambda$ . Large values of  $A_\kappa$  can either push the scalar mass to too large values or lead to a vanishing pseudoscalar mass. Both effects set an upper limit on  $A_\kappa$ . Because  $A_\kappa$  is set at the GUT scale, small starting values of  $A_\kappa$  can turn negative towards the TeV scale, leading to a very light scalar. The correlation between  $\lambda$  and  $A_\kappa$  occurs because for large  $\lambda$  we need larger values of  $A_\kappa$  to keep the pseudoscalar singlet heavy enough.

In the right panel we see that large values of  $A_\kappa$  are only possible for even larger values of  $A_\lambda$ . The scalar and the pseudoscalar singlet mass-squares differ by  $\Delta m^2 = 4(A_\kappa \tilde{\kappa} \mu + \tilde{\kappa}^2 \mu^2)$ , neglecting the subleading term proportional to  $m_Z^2 s_{2\beta} \lambda^2 \tilde{\kappa}$ . For both, the scalar and the pseudoscalar masses to be above zero, this mass difference cannot be larger than the actual mass scale. This means that large  $A_\kappa$  has to be accompanied by even larger  $A_\lambda$ .

## B. Galactic center excess

In the TeV-scale NMSSM a singlino-like LSP with a small Higgsino component can generate the galactic center excess in agreement with the relic density and linked to an enhanced branching ratio  $H_{125} \rightarrow \tilde{\chi}\tilde{\chi}$ . By definition, the NUH-NMSSM contains only a subset of the NMSSM models: the unification condition on  $m_{1/2}$  impacts the range of  $M_1$ , and the stop masses can no longer be set independently of the remaining sfermion masses.

To be consistent with the TeV-scale study we decouple the sfermion sector at  $m_0 = 10$  TeV. This is compatible with the observed Higgs mass, when we adjust  $A_\lambda$  accordingly. Again,  $\tan\beta$  is set to 40, to provide a large coupling between the pseudoscalar Higgs and the down-type quarks. As before,  $\mu$  is set at the SUSY scale of 1 TeV and limited to (150 ... 220) GeV which will be compatible with galactic center excess. To generate a singlino mass around 40 to 50 GeV, we vary  $\tilde{\kappa} = 0.06 \dots 0.18$ , following Eq.(9).

As mentioned in the previous section, gaugino mass unification correlates the bino, wino, and gluino masses. Direct gluino searches set a lower limit of  $m_{1/2} > 500$  GeV [57]. This leads to a heavy wino mass, out of reach for LEP2, and defines a lower bound  $M_1 > 200$  GeV. Both, the bino and wino components of the lightest neutralino become negligible. To compensate for the missing bino component, the Higgsino component needs to be slightly enhanced with respect to the TeV-scale model, leading to the slightly reduced values of  $\mu$  quoted above.

In the TeV-scale case we fix  $A_\lambda$  using Eq.(6). In the NUH-NMSSM this is no longer possible, as  $A_\lambda$  is now defined at the averaged squark mass scale, where also the Higgs masses are computed. We can estimate that for  $\mu = 200$  GeV the value of  $A_\lambda$  at 10 TeV has to be approximately 8 TeV. Neglecting all contributions but  $A_\lambda$  itself in Eq.(30), the value of  $A_\lambda$  increases to around 8.6 TeV when evaluated at the GUT scale. From the global analysis we know that  $A_\kappa$  tends to have the same sign as  $A_\lambda$ . In this case,  $A_\kappa$  further increases the preferred value of  $A_\lambda$  at the GUT scale to around 9 TeV. This fixed value of  $A_\lambda$  now translates into preferred ranges of  $A_\kappa$  and  $\lambda$  via the singlet scalar and pseudoscalar squared mass terms, which need to be larger than zero. Choosing  $\lambda = 0.25 \dots 0.45$  gives  $A_\kappa = (1.5 \dots 5)$  TeV.

In Fig. 6 we show the results of our SFITTER analysis. Just as in the TeV-scale study, we require all points to be compatible with direct detection limits, Higgs mass measurements, and the relic density within the theoretical uncertainty, as given in Tab. I. The chargino masses have to be larger than 103 GeV and the additional contribution to the  $Z$ -width smaller than 2 MeV. All displayed points are consistent with an invisible branching ratio of at least 10%.

As mentioned before, we now study singlino LSPs with a small Higgsino component. On the left hand side of Fig. 6 we show the projection onto the  $\tilde{\kappa} - \mu$  plane. This determines the mass and the composition of the LSP. For the singlino-like LSP the mass increases with  $\mu$  and  $\tilde{\kappa}$ . The allowed region for larger  $\tilde{\kappa}$  corresponds to an LSP mass of 50 to 52 GeV while the strip at  $\tilde{\kappa} \approx 0.11$  corresponds to a neutralino mass of 30 to 40 GeV. In between the two regions, the annihilation via the  $Z$ -pole becomes too efficient. For larger masses the annihilation is too weak to predict the measured relic density. In contrast, towards smaller masses a combination of the  $A_1$ - and  $Z$ -channels gives the correct relic density as well as an annihilation cross section compatible with the galactic center excess.

Apart from its mass, the composition of the LSP plays a key role. For small  $\tilde{\kappa} \approx 0.1$  the sum of the Higgsino components decreases with increasing  $\mu$ , starting from 5% at  $\mu = 205$  GeV and reaching 20% for  $\mu = 160$  GeV. This increased active Higgsino component implies a larger coupling to the Higgs, which leads to an increase of the invisible branching ratio: for  $\mu < 160$  GeV it can reach up to 80%, while for  $\mu > 200$  GeV it drops below

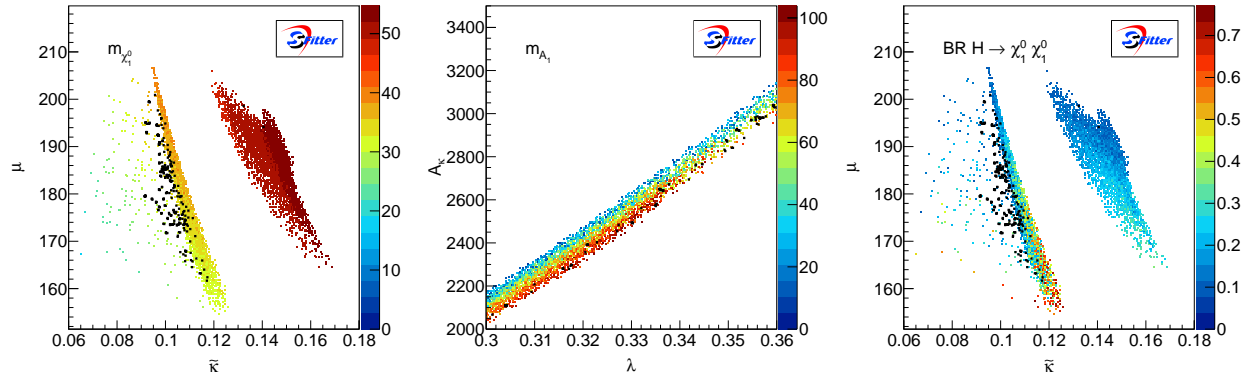


Figure 6: LSP mass, pseudoscalar mediator mass, and invisible Higgs branching ratio in the NUH-NMSSM. As before, we fix  $\tan\beta = 40$ . Like in Fig. 2 all displayed points are compatible with the relic density, Xenon, a chargino mass above 103 GeV, and the correct SM-like Higgs mass. Moreover, they always have an invisible branching ratio  $\text{BR}(H_{125} \rightarrow \tilde{\chi}\tilde{\chi}) > 10\%$ . The black points are consistent with the galactic center excess.

the required 10%. However, from the large coupling to the  $Z$  there follows a negligible annihilation via the pseudoscalar mediator, rendering this region in-compatible with the galactic center excess. Moreover, direct detection limits become relevant for a large  $Z$ -coupling and exclude points with smaller values of  $\mu$ .

In the center panel, we show the  $A_\kappa - \lambda$  plane for a reduced range of  $\lambda = 0.30 \dots 0.36$ . This illustrates the dependence of the lightest pseudoscalar mass on  $A_\kappa$  and  $\lambda$ . From Eq.(7) now directly follows that the  $A_1$ -mass increases with  $\lambda$ , while it decreases with  $A_\kappa$ . Once  $A_\kappa$  becomes too large, the pseudoscalar mass squared crosses zero, limiting the allowed region. For the galactic center excess  $\sigma v$  only reaches sufficiently high values around the on-shell condition for the  $A_1$  funnel. From the discussion of the  $\tilde{\kappa} - \mu$  plane we know that the mass range for neutralinos compatible with the galactic center excess is restricted to  $m_{\tilde{\chi}} = 30 \dots 48$  GeV. This translated into pseudoscalar masses of 60 to 100 GeV.

In the right panel of Fig. 6 the projection on the  $\tilde{\kappa} - \mu$  plane shows the resulting branching ratio for invisible Higgs decays. For the region around  $\tilde{\kappa} \approx 0.15$ ,  $\lambda$  ranges from 0.25 to 0.3, while for  $\tilde{\kappa} \approx 0.11$  the allowed range for  $\lambda$  increases up to 0.45 for  $\mu = 160\text{GeV}$ . Small values of  $\lambda$  result in a small Higgsino component, leading to an invisible branching ratio of 10 to 30% in the region with  $m_{\tilde{\chi}} \approx 50\text{GeV}$ . For the narrow region the lower limit of  $\mu = 155\text{GeV}$  in combination with large values of  $\lambda$  allow for large invisible branching ratios up to 80%.

When we consider only points compatible with the GCE we find

$$\text{BR}(H_{125} \rightarrow \tilde{\chi}\tilde{\chi}) \lesssim 40\% \quad \text{for } \mu = 160 \dots 200 \text{ GeV}, \quad (32)$$

The maximal found branching ratio of 40% is comparable to the results for  $\mu = 220$  GeV in the TeV scale NMSSM where the bino component enhances the coupling. Even though the NUH-NMSSM pushes the neutralino content to a pure singlino-Higgsino state, we can still find regions that are compatible with the relic density, the GCE and a strongly enhanced invisible branching ratio.

#### IV. OUTLOOK

A natural explanation of the Fermi galactic center excess is a light, weakly interacting dark matter particle decaying to a pair of bottom quarks through an  $s$ -channel pseudoscalar. The NMSSM is one of the few models which predict precisely this process.

In the NMSSM framework, the galactic center excess as well as the currently observed relic density can be accommodated with the help of  $Z$ -funnel and  $A_1$ -funnel annihilation [26]. Different preferred parameter spaces can be linked to LHC searches for trileptons [28] or exotic Higgs searches [30]. We show that for a mixed bino-singlino-Higgsino LSP the explanation of the galactic center excess typically predicts large invisible branching ratios of the SM-like Higgs boson. In particular for small  $\mu$  values the invisible branching ratios can reach 50%,

testable with Run I Higgs data. Future LHC analyses, sensitive to invisible branching ratios around 3% [2], cover a large fraction of Higgs decays to a pair of Hooperons. The preferred NMSSM parameters at the TeV scale can also be realized in a unified version of the NMSSM, albeit with larger values of  $M_1$  and slightly reduced  $\mu$ .

### Acknowledgments

AB would like to thank the Heidelberg Graduate School for Fundamental Physics for her PhD funding, LAL for their hospitality and funding during her master thesis work, and the DFG Graduiertenkolleg *Particle Physics beyond the Standard Model* (GK1940). She also would like to thank Laurent Duflot for lively discussions on the phenomenology of the NMSSM and technical support at all stages of the project. TP acknowledges the support by the DFG Forschergruppe *New Physics at the LHC* (FOR2238).

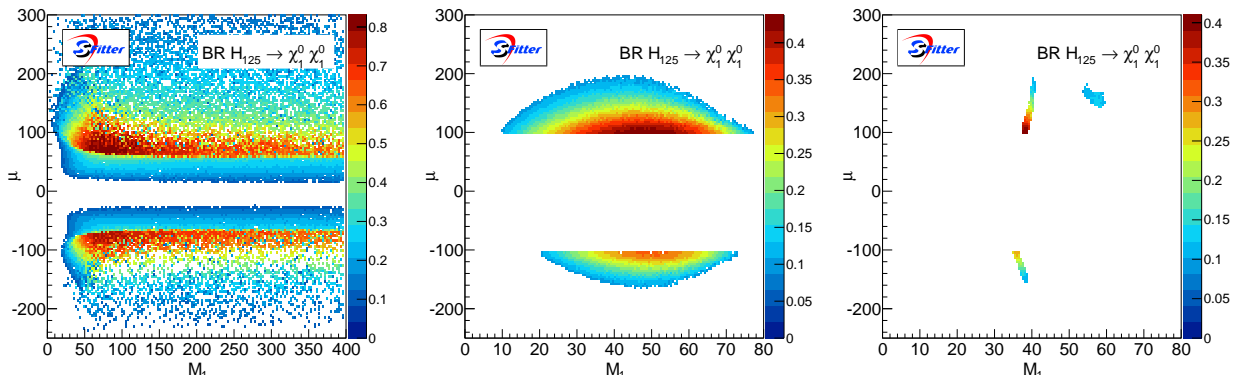


Figure 7: Branching ratio for  $H_{125} \rightarrow \tilde{\chi}_1^0 \tilde{\chi}_1^0$ . From left to right we consecutively apply the constraints: (1)  $m_{H_{125}} = (122 \dots 128)$  GeV and  $\text{BR}_{\text{inv}} > 10\%$ , (2)  $m_{\tilde{\chi}_1^\pm} > 103$  GeV, and (3)  $\Omega_{\tilde{\chi}} h^2 = (0.107 \dots 0.131)$ . The projections are profiled over  $M_2$ , showing the maximal branching ratio.

### Appendix A: Invisible Higgs decays in the MSSM

For the sake of completion we briefly review the constraints on invisible Higgs decays in the MSSM with a SM-like light Higgs. The LSP can be a combination of bino, wino, and Higgsino. First, invisible Higgs decays  $H \rightarrow \tilde{\chi}\tilde{\chi}$  require the LSP to be lighter than 63 GeV. Therefore, at least one of the mass parameters  $\mu$ ,  $M_1$ , and  $M_2$  has to be around 100 GeV or below. The second ingredient is the size of the coupling. Its form given in Eq.(21) requires a mixed Higgsino-gaugino states, which means we again expect to need small values of  $|\mu|$ .

The left panel of Fig. 7 illustrates the dependence of the invisible branching ratio on  $\mu$  and  $M_1$ . We vary the MSSM parameters  $\mu$ ,  $M_1$ , and  $M_2$ . For this example we set the sfermion and gluino masses to 2 TeV, so that they decouple from the electroweak sector, and as before set  $\tan\beta = 40$ . The Higgs-sector parameters  $M_A$ ,  $A_t$  and  $A_\tau$  now have to be carefully chosen to reproduce the observed Higgs mass. For all points shown we require a Higgs invisible branching ratio to be at least 10%.

Without constraints on the chargino mass and dark matter properties the maximal branching ratio exceeds 80%. The relevant parameter space is located around  $|\mu| = 80$  GeV and  $M_1 = 100 \dots 150$  GeV. Away from this region, the LSP is no longer well tempered, reducing the coupling and leading to an invisible branching ratio below 10%.

In the center panel of Fig. 7 we add the LEP limits [22] on the chargino mass. The minimal value of 103 GeV translates into a lower bound  $\mu, M_2 \gtrsim 100$  GeV. The lower bound on  $\mu$  can be seen directly in Fig. 7. The constraint on  $M_2$  works indirectly: it excludes wino LSPs lighter than 63 GeV, which means that a light LSP has to be mainly bino. This is visible as an upper bound  $M_1 < 80$  GeV.

In addition to the LSP mass, we also have to adjust the couplings. The required bino-Higgsino mixing restricts the allowed parameter region to  $M_1 < 80$  GeV and  $|\mu| < 200$  GeV. Constant invisible branching ratios correspond the two half-circles in the center panel of Fig. 7. Without the mass constraints on the chargino and the Higgs we would see two approximately circular shapes centered around  $M_1 \approx 50$  GeV and slightly bigger values of  $|\mu|$ . This reflects the preference for a light, well-tempered LSP with roughly equal bino and Higgsino fractions. In particular the chargino mass limit simply removes the region with  $|\mu| \lesssim 100$  GeV. The maximum invisible branching ratio in the MSSM is 45%.

In the right panel of Fig. 7 we add the Planck measurement of the LSP relic density. In this configuration the annihilation proceeds via an  $s$ -channel  $Z$ -boson. Planck excludes neutralino masses around 45 GeV, where resonant annihilation leads to a too small relic density. Three distinct strips remain compatible with the measured relic density: two with neutralino masses between 35 GeV and 40 GeV, and one between 50 GeV and 55 GeV. However, the latter is excluded by the Xenon100. This additional constraint further reduces the maximal invisible branching ratio

$$\text{BR}(H_{125} \rightarrow \tilde{\chi}\tilde{\chi}) \lesssim 50\% \quad \text{for } \mu = 100 \text{ GeV}, \quad M_1 = 45 \text{ GeV}, \quad (\text{A1})$$

As discussed in Sec. II A, in the absence of a light pseudoscalar mediator we do not consider constraints from the galactic center excess in the MSSM.

Finally, we consider  $Z$ -decays to neutralinos for neutralino masses smaller than 45 GeV. The corresponding partial width adds to the width from  $Z$ -decays into neutrinos, whose SM prediction already exceeds the measured value of  $\Gamma(Z \rightarrow \text{inv})$  by 1.9 MeV. While an invisible Higgs branching ratio of 10% only adds an additional 0.2 MeV to the  $Z$ -width, a Higgs branching ratio of 40% can imply an additional  $Z$ -decay width of 3 MeV. This increases the already existing tension between theory prediction and experimental results for invisible  $Z$ -decays.

- 
- [1] O. J. P. Eboli and D. Zeppenfeld, Phys. Lett. B **495**, 147 (2000); R. M. Godbole, M. Guchait, K. Mazumdar, S. Moretti and D. P. Roy, Phys. Lett. B **571**, 184 (2003).
- [2] C. Bernaciak, T. Plehn, P. Schichtel and J. Tattersall, Phys. Rev. D **91**, no. 3, 035024 (2015).
- [3] G.-C. Cho, K. Hagiwara, J. Kanzaki, T. Plehn, D. Rainwater and T. Stelzer, Phys. Rev. D **73**, 054002 (2006).
- [4] L. Goodenough and D. Hooper, arXiv:0910.2998 [hep-ph]; D. Hooper and L. Goodenough, Phys. Lett. B **697**, 412 (2011); D. Hooper and T. Linden, Phys. Rev. D **84**, 123005 (2011); K. N. Abazajian and M. Kaplinghat, Phys. Rev. D **86**, 083511 (2012) [Phys. Rev. D **87**, 129902 (2013)]; C. Gordon and O. Macias, Phys. Rev. D **88**, no. 8, 083521 (2013) [Phys. Rev. D **89**, no. 4, 049901 (2014)]; O. Macias and C. Gordon, Phys. Rev. D **89**, no. 6, 063515 (2014); K. N. Abazajian, N. Canac, S. Horiuchi and M. Kaplinghat, Phys. Rev. D **90**, no. 2, 023526 (2014); B. Zhou, Y. F. Liang, X. Huang, X. Li, Y. Z. Fan, L. Feng and J. Chang, arXiv:1406.6948 [astro-ph.HE]; S. Murgia (2014), Talk given on Fifth Fermi Symposium, Nagoya, 20-24 October; B. Bertoni, D. Hooper and T. Linden, arXiv:1504.02087 [astro-ph.HE].
- [5] P. A. R. Ade *et al.* [Planck Collaboration], arXiv:1502.01589 [astro-ph.CO].
- [6] M. Ackermann *et al.* [Fermi-LAT Collaboration], Phys. Rev. D **89**, 042001 (2014).
- [7] [ATLAS Collaboration], Phys. Rev. Lett. **112**, 201802 (2014), etc.
- [8] [CMS Collaboration], CMS-PAS-HIG-13-013; CMS-PAS-HIG-13-018. CMS-PAS-HIG-13-028; arXiv:1310.1002 [hep-ex]; CMS-PAS-HIG-14-038; Eur. Phys. J. C **74**, 2980 (2014); [CMS Collaboration], arXiv:1507.00359 [hep-ex].
- [9] J. R. Ellis, J. F. Gunion, H. E. Haber, L. Roszkowski and F. Zwirner, Phys. Rev. D **39**, 844 (1989); M. Drees, Int. J. Mod. Phys. A **4**, 3635 (1989); J. R. Espinosa and M. Quiros, Phys. Lett. B **279**, 92 (1992). U. Ellwanger, M. Rausch de Traubenberg and C. A. Savoy, Phys. Lett. B **315**, 331 (1993).
- [10] for recent reviews see e.g. S. P. Martin, Adv. Ser. Direct. High Energy Phys. **21**, 1 (2010); U. Ellwanger, C. Hugonie and A. M. Teixeira, Phys. Rept. **496**, 1 (2010); M. Maniatis, Int. J. Mod. Phys. A **25**, 3505 (2010).
- [11] for the only other paper with ‘Hooperon’ in the title see A. Alves, S. Profumo, F. S. Queiroz and W. Shepherd, Phys. Rev. D **90**, no. 11, 115003 (2014).
- [12] T. Daylan, D. P. Finkbeiner, D. Hooper, T. Linden, S. K. N. Portillo, N. L. Rodd and T. R. Slatyer, arXiv:1402.6703 [astro-ph.HE]; F. Calore, I. Cholis and C. Weniger, JCAP **1503**, 038 (2015); F. Calore, I. Cholis, C. McCabe and C. Weniger, Phys. Rev. D **91**, no. 6, 063003 (2015).
- [13] H. Goldberg, Phys. Rev. Lett. **50**, 1419 (1983); M. Drees and M. M. Nojiri, Phys. Rev. D **47**, 376 (1993); J. R. Ellis, J. S. Hagelin, D. V. Nanopoulos, K. A. Olive and M. Srednicki, Nucl. Phys. B **238**, 453 (1984); G. Jungman, M. Kamionkowski and K. Griest, Phys. Rept. **267**, 195 (1996); G. Bertone, D. Hooper and J. Silk, Phys. Rept. **405**, 279 (2005).
- [14] for an exceptionally instructive and beautiful set of plots on relic neutralinos see J. Bramante, P. J. Fox, A. Martin, B. Ostdiek, T. Plehn, T. Schell and M. Takeuchi, Phys. Rev. D **91**, no. 5, 054015 (2015).
- [15] P. Agrawal, B. Batell, P. J. Fox and R. Harnik, JCAP **1505**, no. 05, 011 (2015); A. Achterberg, S. Caron, L. Hendriks, R. Ruiz de Austri and C. Weniger, arXiv:1502.05703 [hep-ph].
- [16] S. Henrot-Versille, R. Lafaye, T. Plehn, M. Rauch, D. Zerwas, S. Plaszczynski, B. Rouille d’Orfeuille and M. Spinelli, Phys. Rev. D **89**, no. 5, 055017 (2014).
- [17] T. Cohen and J. G. Wacker, JHEP **1309**, 061 (2013).
- [18] see e.g. A. Fowlie, K. Kowalska, L. Roszkowski, E. M. Sessolo and Y. -L. S. Tsai, Phys. Rev. D **88**, 055012 (2013); C. Streye, G. Bertone, F. Feroz, M. Fornasa, R. Ruiz de Austri and R. Trotta, JCAP **1304**, 013 (2013); B. Bhat-tacherjee, M. Chakraborti, A. Chakraborty, U. Chattopadhyay, D. Das and D. K. Ghosh, arXiv:1305.4020 [hep-ph]; M. Cahill-Rowley, J. Hewett, A. Ismail and T. Rizzo, arXiv:1308.0297 [hep-ph]; O. Buchmüller, R. Cavanaugh, M. Citron, A. De Roeck, M. J. Dolan, J. R. Ellis, H. Flacher and S. Heinemeyer *et al.*, Eur. Phys. J. C **72**, 2243 (2012); etc.
- [19] K. Griest and D. Seckel, Phys. Rev. D **43**, 3191 (1991); S. Mizuta and M. Yamaguchi, Phys. Lett. B **298**, 120 (1993); J. R. Ellis, T. Falk and K. A. Olive, Phys. Lett. B **444**, 367 (1998).
- [20] C. Boehm, A. Djouadi and M. Drees, Phys. Rev. D **62**, 035012 (2000).

- [21] P. Binetruy, G. Girardi and P. Salati, Nucl. Phys. B **237**, 285 (1984); S. Mizuta and M. Yamaguchi, Phys. Lett. B **298**, 120 (1993);
- [22] ALEPH Collaboration, Phys. Lett. B526 (2002) 206, Phys. Lett. B583 (2004) 247; DELPHI Collaboration, Eur. Phys. J. C31 (2003) 421-479; L3 Collaboration, Phys. Lett. B580 (2004) 37; OPAL Collaboration, Eur. Phys. J. C32 (2004) 453-473; ALEPH Collaboration, Phys. Lett. B537 (2002) 5-20; OPAL Collaboration, Phys. Lett. B545 (2002) 272-284; ALEPH Collaboration, Phys. Lett. B533 (2002) 223-236; L3 Collaboration, Phys. Lett. B471 (1999) 308-320. LEP2 SUSY Working Group, ALEPH, DELPHI, L3 and OPAL experiments, <http://lepsusy.web.cern.ch/lepsusy>
- [23] D. K. Ghosh, S. Mondal and I. Saha, JCAP **1502**, no. 02, 035 (2015); A. Berlin, S. Gori, T. Lin and L. T. Wang, arXiv:1502.06000 [hep-ph].
- [24] A. Berlin, D. Hooper and S. D. McDermott, Phys. Rev. D **89**, no. 11, 115022 (2014); M. Abdullah, A. DiFranzo, A. Rajaraman, T. M. P. Tait, P. Tanedo and A. M. Wijangco, Phys. Rev. D **90**, no. 3, 035004 (2014); C. Balazs, T. Li, C. Savage and M. White, arXiv:1505.06758 [hep-ph].
- [25] for general aspects of the singlet/singlino in the NMSSM see e.g. U. Ellwanger and C. Hugonie, Eur. Phys. J. C **5**, 723 (1998); A. Dedes, C. Hugonie, S. Moretti and K. Tamvakis, Phys. Rev. D **63**, 055009 (2001); S. Y. Choi, D. J. Miller and P. M. Zerwas, Nucl. Phys. B **711**, 83 (2005); V. Barger, P. Langacker and G. Shaughnessy, Phys. Lett. B **644**, 361 (2007); K. Cheung and T. J. Hou, Phys. Lett. B **674**, 54 (2009); O. Stal and G. Weiglein, JHEP **1201**, 071 (2012) D. G. Cerdeno, P. Ghosh, C. B. Park and M. Peiro, JHEP **1402**, 048 (2014); U. Ellwanger and A. M. Teixeira, JHEP **1410**, 113 (2014).
- [26] M. Cahill-Rowley, J. Gainer, J. Hewett and T. Rizzo, JHEP **1502**, 057 (2015); T. Gherghetta, B. von Harling, A. D. Medina, M. A. Schmidt and T. Trott, Phys. Rev. D **91**, 105004 (2015); R. Enberg, S. Munir, C. P. d. l. Heros and D. Werder, arXiv:1506.05714 [hep-ph]; J. Cao, L. Shang, P. Wu, J. M. Yang and Y. Zhang, arXiv:1506.06471 [hep-ph].
- [27] J. Huang, T. Liu, L. T. Wang and F. Yu, Phys. Rev. D **90**, no. 11, 115006 (2014).
- [28] J. Guo, J. Li, T. Li and A. G. Williams, Phys. Rev. D **91**, no. 9, 095003 (2015); J. Cao, L. Shang, P. Wu, J. M. Yang and Y. Zhang, Phys. Rev. D **91**, no. 5, 055005 (2015).
- [29] X. J. Bi, L. Bian, W. Huang, J. Shu and P. F. Yin, arXiv:1503.03749 [hep-ph].
- [30] C. Cheung, M. Papucci, D. Sanford, N. R. Shah and K. M. Zurek, Phys. Rev. D **90**, no. 7, 075011 (2014).
- [31] J. Kozaczuk and T. A. W. Martin, JHEP **1504**, 046 (2015).
- [32] for a Higgs portal linked to invisible decays see e.g. V. Silveira and A. Zee, Phys. Lett. B **161**, 136 (1985); J. McDonald, Phys. Rev. D **50**, 3637 (1994); C. P. Burgess, M. Pospelov and T. ter Veldhuis, Nucl. Phys. B **619**, 709 (2001); R. Schabinger and J. D. Wells, Phys. Rev. D **72**, 093007 (2005) B. Patt and F. Wilczek, hep-ph/0605188. R. Barbieri, T. Gregoire and L. J. Hall, hep-ph/0509242; M. H. G. Tytgat, PoSIDM **2010**, 126 (2011); C. Englert, T. Plehn, D. Zerwas and P. M. Zerwas, Phys. Lett. B **703**, 298 (2011); M. Pospelov and A. Ritz, Phys. Rev. D **84**, 113001 (2011) X. -G. He and J. Tandean, Phys. Rev. D **84**, 075018 (2011); P. J. Fox, R. Harnik, J. Kopp and Y. Tsai, Phys. Rev. D **85**, 056011 (2012); I. Low, P. Schwaller, G. Shaughnessy and C. E. M. Wagner, Phys. Rev. D **85**, 015009 (2012); C. Englert, T. Plehn, M. Rauch, D. Zerwas and P. M. Zerwas, Phys. Lett. B **707**, 512 (2012); A. Djouadi, O. Lebedev, Y. Mambrini and J. Quevillon, Phys. Lett. B **709**, 65 (2012); B. Batell, S. Gori and L. T. Wang, JHEP **1206**, 172 (2012); S. Baek, P. Ko and W. I. Park, Phys. Rev. D **90**, no. 5, 055014 (2014).
- [33] J. R. Ellis, J. F. Gunion, H. E. Haber, L. Roszkowski and F. Zwirner, Phys. Rev. D **39**, 844 (1989); M. Drees, Int. J. Mod. Phys. A **4**, 3635 (1989); F. Franke and H. Fraas, Int. J. Mod. Phys. A **12**, 479 (1997); D. J. Miller, R. Nevzorov and P. M. Zerwas, Nucl. Phys. B **681**, 3 (2004); U. Ellwanger and C. Hugonie, Phys. Lett. B **623**, 93 (2005); G. Degrassi and P. Slavich, Nucl. Phys. B **825**, 119 (2010).
- [34] M. Masip, R. Munoz-Tapia and A. Pomarol, Phys. Rev. D **57**, R5340 (1998); M. A. Diaz, T. A. ter Veldhuis and T. J. Weiler, Phys. Rev. D **54**, 5855 (1996); U. Ellwanger and C. Hugonie, Eur. Phys. J. C **25**, 297 (2002); M. D. Goodsell, K. Nickel and F. Staub, Phys. Rev. D **91**, no. 3, 035021 (2015).
- [35] [ATLAS and CMS Collaborations], Phys. Rev. Lett. **114**, 191803 (2015).
- [36] for a short history of MSSM studies see e.g. M. S. Carena, J. R. Espinosa, M. Quiros and C. E. M. Wagner, Phys. Lett. B **355**, 209 (1995); H. E. Haber, R. Hempfling and A. H. Hoang, Z. Phys. C **75**, 539 (1997); S. Heinemeyer, W. Hollik and G. Weiglein, Eur. Phys. J. C **9**, 343 (1999); G. Degrassi, S. Heinemeyer, W. Hollik, P. Slavich and G. Weiglein, Eur. Phys. J. C **28**, 133 (2003); P. Kant, R. V. Harlander, L. Mihaila and M. Steinhauser, JHEP **1008**, 104 (2010); T. Hahn, S. Heinemeyer, W. Hollik, H. Rzehak and G. Weiglein, Phys. Rev. Lett. **112**, no. 14, 141801 (2014); E. Bagnaschi, R. V. Harlander, S. Liebler, H. Mantler, P. Slavich and A. Vicini, JHEP **1406**, 167 (2014); G. Degrassi, S. Di Vita and P. Slavich, Eur. Phys. J. C **75**, no. 2, 61 (2015).
- [37] G.W. Bennett et al., Phys. Rev. Lett. **89**, 101804 (2002); Erratum *ibid.* Phys. Rev. Lett. **89**, 129903 (2002); G.W. Bennett et al., Phys. Rev. Lett. **92**, 161802 (2004); G.W. Bennett et al., Phys. Rev. D **73**, 072003 (2006); Particle Data Group <http://pdg.lbl.gov/2014/reviews/rpp2014-rev-g-2-muon-anom-mag-moment.pdf>
- [38] CLEO Collaboration, Phys. Rev. Lett. **87**, 251807 (2001); BaBar Collaboration, Phys. Rev. D **86**, 112008 (2012); Belle Collaboration, Phys. Rev. Lett. **103**, 241801 (2009); Particle Data Group <http://pdg.lbl.gov/2014/reviews/rpp2014-rev-b-meson-prod-decay.pdf>
- [39] [LHCb Collaboration], Phys. Rev. Lett. **110**, 021801 (2013); CMS Collaboration, Phys. Rev. Lett. **111**, 101804

- (2013); CMS and LHCb Collaborations, *Nature* **522**, 68 (2015).
- [40] D. Asner *et al.* [Heavy Flavor Averaging Group Collaboration], arXiv:1010.1589 [hep-ex].
- [41] ALEPH Collaboration, EPJ C14 1; Delphi Collaboration, EPJ C16 371; L3 Collaboration, EPJ C16 1; OPAL Collaboration, EPJ C19 587; Particle Data Group: <http://pdg.lbl.gov/2014/listings/rpp2014-list-z-boson.pdf>
- [42] Tevatron Electroweak Working Group [CDF and D0 Collaborations], arXiv:1407.2682 [hep-ex]; [ATLAS and CDF and CMS and D0 Collaborations], arXiv:1403.4427 [hep-ex]; K. Kröniger, A. B. Meyer and P. Uwer, arXiv:1506.02800 [hep-ex]; Particle Data Group: <http://pdg.lbl.gov/2014/reviews/rpp2014-rev-top-quark.pdf>
- [43] E. Aprile *et al.* [XENON100 Collaboration], *Phys. Rev. Lett.* **107**, 131302 (2011); E. Aprile *et al.* [XENON100 Collaboration], *Phys. Rev. Lett.* **109**, 181301 (2012). We use the conservative Xenon100 results, but in our bottom line the only effects from including the Lux limits is a shift in  $\mu$  and its correlations.
- [44] R. Lafaye, T. Plehn and D. Zerwas, arXiv:hep-ph/0404282; R. Lafaye, T. Plehn, M. Rauch and D. Zerwas, *Eur. Phys. J. C* **54**, 617 (2008).
- [45] C. Adam, J. -L. Kneur, R. Lafaye, T. Plehn, M. Rauch and D. Zerwas, *Eur. Phys. J. C* **71**, 1520 (2011); E. Turlay, R. Lafaye, T. Plehn, M. Rauch and D. Zerwas, *J. Phys. G* **38**, 035003 (2011).
- [46] for the similar FITTINO approach see e.g. P. Bechtle, K. Desch and P. Wienemann, arXiv:hep-ph/0412012; P. Bechtle, T. Bringmann, K. Desch, H. Dreiner, M. Hamer, C. Hensel, M. Krämer and N. Nguyen *et al.*, *JHEP* **1206** (2012) 098.
- [47] A. Höcker, H. Lacker, S. Laplace and F. Le Diberder, *Eur. Phys. J. C* **21**, 225 (2001).
- [48] U. Ellwanger, J. F. Gunion and C. Hugonie, *JHEP* **0502** (2005) 066 [hep-ph/0406215]. U. Ellwanger and C. Hugonie, *Comput. Phys. Commun.* **175**, 290 (2006); G. Belanger, F. Boudjema, C. Hugonie, A. Pukhov and A. Semenov, *JCAP* **0509**, 001 (2005); U. Ellwanger and C. Hugonie, *Comput. Phys. Commun.* **177**, 399 (2007).
- [49] G. Belanger, F. Boudjema, P. Brun, A. Pukhov, S. Rosier-Lees, P. Salati and A. Semenov, *Comput. Phys. Commun.* **182**, 842 (2011).
- [50] R. Lafaye, T. Plehn, M. Rauch, D. Zerwas and M. Dührssen, *JHEP* **0908**, 009 (2009); M. Klute, R. Lafaye, T. Plehn, M. Rauch and D. Zerwas, *Phys. Rev. Lett.* **109**, 101801 (2012); D. Lopez-Val, T. Plehn and M. Rauch, *JHEP* **1310**, 134 (2013).
- [51] A. Djouadi, J. Kalinowski and M. Spira, *Comput. Phys. Commun.* **108**, 56 (1998); M. Mühlleitner, A. Djouadi and Y. Mambrini, arXiv:hep-ph/0311167; A. Djouadi, M. M. Mühlleitner and M. Spira, *Acta Phys. Polon. B* **38**, 635 (2007).
- [52] A. Djouadi, J. -L. Kneur and G. Moultaka, *Comput. Phys. Commun.* **176**, 426 (2007); G. Brooijmans *et al.*, arXiv:1203.1488 [hep-ph].
- [53] S. Heinemeyer, W. Hollik, A. M. Weber and G. Weiglein, *JHEP* **0804**, 039 (2008). A. Weber, private communication.
- [54] T. Corbett, O. J. P. Eboli, D. Goncalves, J. Gonzalez-Fraile, T. Plehn and M. Rauch, arXiv:1505.05516 [hep-ph].
- [55] L. E. Ibañez, *Phys. Lett. B* **118**, 73 (1982); J. R. Ellis, D. V. Nanopoulos and K. Tamvakis, *Phys. Lett. B* **121**, 123 (1983); L. Alvarez-Gaumé, J. Polchinski and M. B. Wise, *Nucl. Phys. B* **221**, 495 (1983); K. Inoue, A. Kakuto, H. Komatsu and S. Takeshita, *Prog. Theor. Phys.* **68**, 927 (1982) [Erratum-ibid. **70**, 330 (1983)]; A. H. Chamseddine, R. Arnowitt and P. Nath, *Phys. Rev. Lett.* **49**, 970 (1982).
- [56] A. Djouadi, U. Ellwanger and A. M. Teixeira, *Phys. Rev. Lett.* **101**, 101802 (2008).
- [57] [ATLAS Collaboration], *JHEP* **1409**, 176 (2014).